Memoirs of the Faculty of Engineering, Nagoya University
Vol.43, No.2 (1991)

THREE-DIMENSIONAL CALCULATION OF RADIATIVE FIELD IN HYPERSONIC AIR SHOCK LAYERS

Akihiro SASOH*, Xin-Yu CHANG, Toshiyuki MURAYAMA‡ and Toshi FUJIWARA

Department of Aeronautical Engineering

(Received October 31, 1991)

Abstract

The method of numerical calculation of three-dimensional radiative transfer from nonequilibrium air shock layers over a body is presented with some reviews on radiative transfer and molecular physics. A numerical technique, which reduces the necessitating memory size of a computational resource, thereby enabling one to conduct three-dimensional calculation, has been developed. This method is applied to radiative heat transfer problems under a reentry condition. The radiative structure of the hypersonic air shock layer generated around a body is closely related to the thermally nonequilibrium structure of the shock layer. A radiative heat transfer which is comparable with the convective one is calculated at such a high Mach number as 35 at an altitude 70 km. This result suggests the importance of radiative heat transfer in thermal design of a reentry vehicle.

Contents

* Currently Associate Professor, Institute of Fluid Science, Tohoku University.
‡ Currently Toyota Motor Corporation.

Nomenclature

A = coupling constant, Eq. 105 $[m^{-1}]$
$A_{n'n''}$ = Einstein transition probability of spontaneous emission (Einstein's A-coefficient) $[s^{-1}]$
A_ν = spectral wall absorptivity [dimensionless]
a = coefficient defined by Eq. 94
B_e = constant, Eq. 64 $[m^{-1}]$
$B_{n''n'}$ = Einstein transition probability of absorption (Einstein's B-coefficient) $[m^3 \cdot m^{-1}/(J \cdot s)]$
B_ν = one of rotational constants, Eq. 63 $[m^{-1}]$
b = coefficient defined by Eq. 95
c = 3.00×10^8 [m/s], speed of light

D_e = constants, Eq. 66 $[m^{-1}]$
D_u = one of rotational constants, Eq. 65 $[m^{-1}]$
$d\omega$ = infinitesimal solid angle $[sr]$
E = energy $[J]$
$E_{ionization}$ = inonization energy $[J]$
E_n = electronic potential energy at n-level $[J]$
e = charge of electron $[C]$
= total energy density, Eq. 99 $[J/m^3]$
e_w = wall emissivity [dimensionless]
F = rotational energy $[m^{-1}]$
f_{abs} = oscillator strength (f-number) of absorption [dimensionless]
f_{emis} = oscillator strength (f-number) of emission [dimensionless]
$f(v)$ = velocity distribution function
G = vibrational energy $[m^{-1}]$
g = degeneracy [dimensionless]
h = 6.626×10^{-34} [J · s], Planck's constant
I = moment of inertia $[kg \cdot m^2]$
$I_{b\lambda}$ = spectral radiant intensity of balckbody with respect to wave-length interval, $[W/(m^2 \cdot m \cdot sr)]$
I_{bv} = spectral radiant intensity of blackbody with respect to wavenumber interval, $[W/(m^2 \cdot m^{-1} \cdot sr)]$
$I_{sm,j}$ = smoothed radiant intensity of j-th band $[W/(m^2 \cdot m^{-1} \cdot sr)]$
$I_{sm,j,nm}$ = smoothed radiant intensity of j-th band which corresponds to m-th outermost boundary $[W/(m^2 \cdot m^{-1} \cdot sr)]$
I_v = spectral radiant intensity $[W/(m^2 \cdot m^{-1} \cdot sr)]$
I_v^0 = spectral radiant intensity incident on medium $[W/(m^2 \cdot m^{-1} \cdot sr)]$
$I_{v,isotropic}$ = spectral radiant intensity when radiative emission is isotropic $[W/(m^2 \cdot m^{-1} \cdot sr)]$
i_{max} = maximum number of chemical species [dimensionless]
J = emission power $[W/m^3]$
= rotational quantum number [dimensionless]
j = serial number of band [dimensionless]
j_v = spectral emission coeffcient $[W/(m^3 \cdot m^{-1} \cdot sr)]$ or $[W/(m^3 \cdot \mu m^{-1} \cdot sr)]$
K = quantum number of total angular momentum apart from electron spin [dimensionless]
$K_{A,n'n''}$ = rate coefficient of transition from n′- to n″- state of A-species $[m^3/s]$
k = 1.38×10^{-23}[J/K], Boltzmann's constant
k_{ip} = rate coefficient of inverse-predissociation $[m^3/s]$
k_p = rate coefficient of predissociation $[s^{-1}]$
L = length of light path through a volume element $[m]$
L_a = line shape function of absorption
L_e = line shape function of emission
M = molecular weight [g/mol]
= Mach number [dimensionless]
m = serial number of outermost boundary surface [dimensionless]
= molecular mass [kg]
m_e = 9.1×10^{-31} [kg], electron mass
N = number density $[m^{-3}]$
N_{array} = number of division of wavenumber [dimensionless]

N_{band} = number of band [dimensionless]
N_{ex} = upper limit of exponent [dimensionless]
n = serial number of body surface [dimensionless]
= (electronic) principal quantum number [dimensionless]
$\mathbf{n}$ = unit vector which is externally normal to wall [dimensionless]
n_A = number density of A-species $[m^{-3}]$
P = emission power $[W/m^3]$
p = pressure, Eq. 75 [atom]
Q = partition function [dimensionless]
q_r = radiative heat flux to wall $[W/m^2]$
$q_{v'v''}$ = Franck-Condon factor [dimensionless]
$\mathbf{R}$ = position vector $[m]$
$\mathbf{R}_{n'n''}$ = matrix element of transition $[C \cdot m]$
R_ν = spectral wall reflectivity [dimensionless]
r = internuclear distance $[m]$
S = one-sided integrated energy flux $[W/m^2]$
= quantum number of resultant of electron spins [dimensionless]
$S^{J'\Lambda'}_{J''\Lambda''}$ = line intensity factor [dimensionless]
$S_{b\nu}$ = one-sided spectral energy flux of blackbody $[W/(m^2 \cdot m^{-1})]$
S_ν = one-sided spectral energy flux $[W/(m^2 \cdot m^{-1})]$
T = temperature $[K]$
= heavy particle translational-rotational temperature used in two-temperature model $[K]$
T_e = electron translational temperature $[K]$
T_{el} = electronic energy $[m^{-1}]$
T_v = vibrational temperature $[K]$
T_{ve} = vibrational-electron tranlational temperature used in two-temperature model $[K]$
u_ν = spectral radiant energy density $[J/(m^3 \cdot m^{-1})]$
v = velocity $[m/s]$
= vibrational quantum number [dimensionless]
w_g = Gaussian line width $[m]$
w_l = Lorentzian line width $[m]$
w_ν = Voigt line width $[m]$
x, y = coordinate $[m]$
x_e, y_e, z_e = constants, Eq. 68 [dimensionless]
Y = Eq. 105 [dimensionless]
Z_1, Z_2 = Eqs. 104 and 103, respectively [dimensionless]
α_e = emissivity of gas, Eq. 10 [dimensionless]
= constant, Eq. 63 $[m^{-1}]$
α_t = transmissivity of gas, Eq. 11 [dimensionless]
β_e = constnat, Eq. 65 $[m^{-1}]$
ΔE_{el} = difference in electronic energy $[J]$
ΔE_{rot} = difference in rotational energy $[J]$
ΔE_{vib} = difference in vibrational energy $[J]$
$\Delta\lambda$ = line width at half-height $[m]$
$\Delta\nu_j$ = band width of j-th band $[m^{-1}]$
ϵ_0 = 8.85×10^{-12} [F/m], permittivity in vacuum
κ_ν = spectral absorption coefficient $[m^{-1}]$

Λ = Quantum number of electron orbital angular momentum along internuclear axis [dimensionless]
λ = $1/\nu$, wavelength $[m]$
ν = wavenumber $[m^{-1}]$
$\nu_{l,j}$ = wavenumber lower limit of j-th band $[m^{-1}]$
$\nu_{u,j}$ = wavenumber upper limit of j-th band $[m^{-1}]$
$\nu_{n'n''}$ = wavenumber of radiation by transition from n′- to n″ energy level $[m^{-1}]$
Σ = quantum number of electronic spin component along internuclear axis [dimensionless]
σ = $5.67 \times 10^{-8}[W/(m^2 \cdot K^4)]$, Stefan-Boltzmann constant
σ_c = cross-section of radiative capture $[m^2]$
σ_p = cross-section of photoionization $[m^2]$
σ_1, σ_2 = collision diameter of molecule 1 and 2, respectively $[m]$
$\tau_\nu(\Delta x)$ = optical thickness at a wavenumber ν corresponding to a physical thickness Δx [dimensionless]
$\boldsymbol{\omega}$ = pointing vector
ω_e = wave number of vibration $[m^{-1}]$

Subscript

av = average
CL = center of line spectrum
e = electron
l = lower level
u = upper level
$+$ = ion
$+,-,g,u$ see Sec.3.2.2.

Superscript

′ = upper state
″ = lower state
¯ (directly over quantity) mean value

1. Introduction

In designing a space vehicle, thermal protection under reentry condition is one of the most important problems. This problem becomes serious, in particular, to so-called AOTV (aero-assisted orbital transfer vehicle) which is originally proposed by London.[1] On one hand, it positively utilizes the atmosphere for braking. On the other hand, it experiences much heat transfer from a hypersonic shock layer generated around the vehicle.

The typical cause of heating over a reentry vehicle is convective heat transfer. It has been relatively well studied and can be quantitatively estimated in experimental and/or numerical ways. Moreover, some methods to reduce convective heat transfer, e.g., the bluntness effect and gas injection from the wall, have been found effective and practically conducted.

However, it has been pointed out that, at a flight Mach number of as high as 25 or higher, radiative heat transfer cannot be neglected.[2),3),4)] Generally speaking, a shock layer generated at such a high Mach number at an altitude of about 70 km is in chemically and thermally nonequilibrium: The rate of each chemical reaction is finite, and is not necessarily

equal to the rate of the backward reaction. All the temperatures which correspond to a translational or an internal mode of molecules are not necessarily equal. In particular, it is possible that the molecules are in electronical nonequilibrium.

Naturally, the radiation emitted from such a nonequilibrium shock layer depends strongly on wavelength; it is the sum of the radiations caused by radiative transitions of the respective species. A simple approximation, such as the gray medium approximation, is not sufficient in order to quantitatively estimate the radiative heat transfer. Instead, one first needs to calculate the flowfield in the nonequilibrium shock layer generated around a body. Next, the radiative properties are to be calculated by superimposing the contributions of the respective species. Finally, one needs to conduct radiative transfer calculation; practically three-dimensional calculation is necessary. Due to strong wavelength dependence mentioned above, a huge amount of spectral data is needed. This requires a large memory size of a computational resource and a long computational period. It seems that, at the present state of art, the method of calculating the radiative field in a shock layer which contains such complicated phenomena as described above has not been established.

The purpose of this paper is to develop the method of calculating the radiative field in a hypersonic nonequilibrium shock layer, and to study the effect of the flowfield condition on the radiative field. The method developed here is wavelength-dependent and three-dimensional. Also, it takes the effect of self-absorption by the shock layer into account.

2. Radiative Transfer through Gaseous Medium

Generally speaking, a high temperature gaseous medium emits and absorbs radiant energy due to transitions of electronic, vibrational and rotational energy levels of molecules. The molecular processes which result in radiative emission and absorption will be discussed in detail in Chap. 3. In this chapter, fundamental equations and parameters on radiative transfer are reviewed. Note that the radiative transfer in a medium is equivalent to the flow of photons whose wavenumber (or wavelength) corresponds to the difference between the energies at the upper and lower levels of a transition.

2. 1. Fundamental Equation of Radiative Transfer

In order to obtain a fundamental equation which describes radiative transfer through a non-uniform media, let us consider a volume element of an infinitesimal thickness (see Fig. 2.1). Here all the flow properties in the element are assumed to be uniform. A light ray in the x-direction is incident at point A, and is transmitted through the element, emanating at point B. In this figure, $I_\nu(x)$ denotes the radiant intensity at point A. Radiant intensity is radiative energy which passes through a unit area normal to the ray per unit time, per unit wavenumber interval and per unit solid angle $[W/(m^2 \cdot m^{-1} \cdot sr)]$. Although it is a function both of direction (vector ω) and of wavenumber at a point, it will hereafter be denoted by $I_\nu(x)$ or I_ν for simplicity.

Note here that I_ν is not a vector quantity but a scalar one. A vector quantity, e.g. a velocity, is totally determined by its direction and magnitude. It is a single-valued function with respect to space. Yet, this is not the case with radiant intensity. Typical examples of a radiant intensity are shown in Figs. 2.2. If there exists just a ray parallel to an axis, the radiant intensity in the direction of the axis is infinite (however, becomes finite by integrating with respect to solid angle), and the other components are equal zero (Fig. 2.2(a)). In contrast, in the case of isotropic radiation (Fig. 2.2(b)), radiant intensities in any directions are all the same.

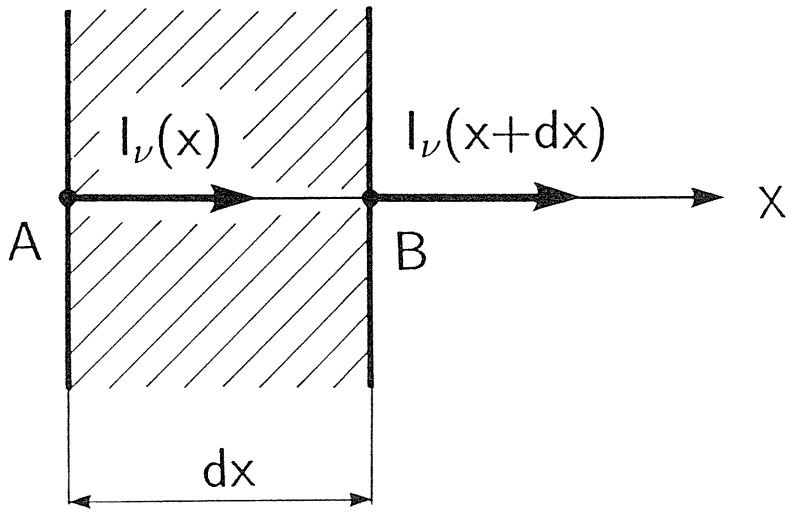

Fig. 2. 1. Ray of light through a medium of an infinitesimal thickness.

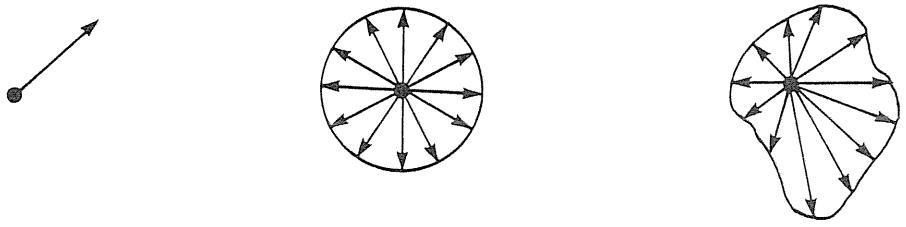

Fig. 2. 2. Examples of directional distribution of radiant intensity (two-dimensional);
(a) One-directional distribution, (b) Isotropic distribution, (c) General distribution.

The general distribution of radiant intensity is shown in Fig. 2.2(c). Radiant intensities in different directions are independent of each other. They are individually determined only after solving the radiative transfer equation. They cannot be united into a single quantity; the magnitude of radiant intensity is a function of the direction of a ray.

If the medium in the element absorbs a fraction of the radiant energy incident on the element, the radiant intensity at point B in Fig. 2.1 is decreased . The effect of the absorption is expressed using 'absorption coefficient.' It is the reciprocal of the mean free path of a photon; a photon in the ray is absorbed after traveling, in average, this distance. The unit of absorption coefficient is $[m^{-1}]$. In the absence of radiative emission in the element, the radiant intensity at point B is related to that at point A by the following differential equation;

$$\frac{dI_\nu}{dx} = -\kappa_\nu I_\nu \ . \tag{1}$$

Here, κ_ν denotes the absorption coefficient which is the function of wavenumber.

When the volume element emits radiation, the radiant intensity is increased at point B. The radiative energy isotropically emitted at a wavenumber ν per unit volume, per unit time, per unit wavenumber interval and per unit solid angle is referred to as 'spectral emission coefficient,' and is denoted by j_ν. Radiative transfer with radiative emission and without absorption is expressed by

$$\frac{dI_\nu}{dx} = j_\nu \ . \tag{2}$$

The general form of the fundamental equation for radiative transfer is rewritten, such as,[5),6)]

$$\frac{1}{c}\frac{\partial I_\nu}{\partial t} + \omega \cdot \nabla I_\nu = j_\nu - \kappa_\nu I_\nu \ . \tag{3}$$

Since the speed of light is much higher than that of flow particles, the first term in the left-hand side is neglected even in an unsteady flow case. Therefore, the following fundamental equation is usually used.

$$\omega \cdot \nabla I_\nu = j_\nu - \kappa_\nu I_\nu \ . \tag{4}$$

2. 2. Ray of Light through Gaseous Medium

Solving Eq. 4 in a one-dimensional case (see Fig. 2.3) yields[5)]

$$I_\nu(x) = \int_{x_0}^{x} exp[-\int_{x'}^{x} \kappa_\nu dx''] j_\nu dx' + I_\nu(x_0) exp[-\int_{x_0}^{x} \kappa_\nu dx'] \tag{5}$$

Here,

$$\tau_\nu(\Delta x) \equiv \int_{x_0}^{x} \kappa_\nu dx' \ , \tag{6}$$

$$\Delta x \equiv x - x_0 \ . \tag{7}$$

$\tau_\nu(\Delta x)$ is called 'spectral optical thickness' which corresponds to a physical distance Δx. It is a function of wavenumber ν. If $\tau_\nu(\Delta x)$ is much larger than unity, the medium is called 'optically thick;' most of the light at the wavenumber incident on the medium is absorbed in it. In contrast, when $\tau_\nu(\Delta x)$ is much smaller than unity, the medium is called 'optically thin;' most of the light at the wavenumber incident on the medium is transmitted through it.

When both the emission and absorption coefficients are constant in the medium, the optical thickness becomes the product of the absorption coefficient and physical thickness of the medium.

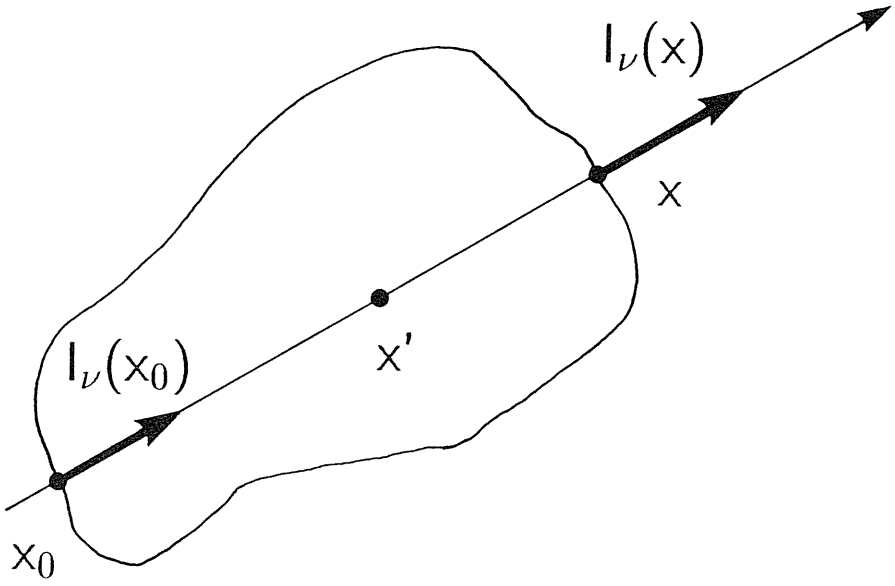

Fig. 2. 3. Ray of light through a non-uniform medium.

$$\tau_\nu(\Delta x) = \kappa_\nu \Delta x \ . \tag{8}$$

In this case, Eq. 5 is transformed into

$$I_\nu(x) = \alpha_{e,\nu} \frac{j_\nu}{\kappa_\nu} + \alpha_{t,\nu} I_\nu(x_0) \ , \tag{9}$$

$$\alpha_{e,\nu} \equiv 1 - e^{-\kappa_\nu \Delta x} \ , \tag{10}$$

$$\alpha_{t,\nu} \equiv e^{-\kappa_\nu \Delta x} \ . \tag{11}$$

$\alpha_{t,\nu}$ is usually called 'transmissivity.' The $e^{-\kappa_\nu \Delta x}$ of the radiant intensity incident at $x=x_0$ is transmitted through the medium. α_e is called the 'emissivity' of gas.

The effect of induced emission on radiative transfer is included by substituting κ_ν by[5)]

$$\kappa'_\nu = \kappa_\nu (1 - e^{-\frac{hc\nu}{kT}}) \ . \tag{12}$$

In this paper, although the superscript ' will hereafter be omitted for simplicity, the effect of spontaneous emission will always be taken into account.

2. 3. *Radiative Transfer in Limiting Cases*

2. 3. 1. *Optically thick case*

When an optical thickness is much larger than unity, $\alpha_{e,\nu}$ given by Eq. 10 becomes close to unity, and $\alpha_{t,\nu}$ given by Eq. 11 becomes negligible. Hence, from Eq. 9, in this case radiant intensity is related to emission and absorption coefficients as follows;

$$j_\nu = \kappa_\nu I_\nu \ . \tag{13}$$

Eq. 13 implies that the radiative energy emitted in a medium is equal to that is absorbed. Substituting Eq. 13 into Eq. 4,

$$\frac{dI_\nu}{dx} = 0 \ . \tag{14}$$

Eq. 14 gives the condition of 'radiative equilibrium'. In this case, the radiant intensity becomes the black body intensity given by

$$I_{b\nu} = \frac{2hc^2\nu^3}{e^{\frac{hc\nu}{kT}} - 1} \ . \tag{15}$$

Therefore, in radiative equilibrium,

$$j_\nu = \kappa_\nu I_{b\nu} \tag{16}$$

The above relationship is called 'Kirchhoff's law.' It is derived from the detailed balancing of radiative processes[5].

2. 3. 2. *Optically thin case*

Another limiting case is an optically thin case. When an optical thickness is much smaller than unity, Eq. 9 is approximately transformed into

$$I_\nu(x) = j_\nu \Delta x + I_\nu(x_0) \ . \tag{17}$$

In this case, the radiant intensity at x=x is the sum of that incident at x=x_0 and that generated by radiative emission through the light path from x=x_0 to x. There is no self-absorption effect. Eq. 17 is a linear equation with respect to radiant intensity. If the distribution of j_ν is known, radiative field can easily be solved.

2. 4. *Other Relations and Parameters on Radiative Transfer*

There are several other relations and parameters which are closely related to radiative transfer. Although all the following items are not necessarily needed in this study, they are listed with brief explanations for convenience.

2. 4. 1. Relationship between wavenumber and wavelength

In order to solve a radiative heat transfer probelm, it is suitable to relate a spectral radiant energy with a wavenumber; the intergrating spectral radiant energy with respect to wavenumber directly results in radiant energy. However, in order to graphically express the spectra of emission and absorption coefficients, they are usually expressed as functions of wavelength. These custom sometimes seems to cause some unnecessary complication.

Wavenumber is transformed into wavelength by

$$\lambda = \frac{1}{\nu} \tag{18}$$

Hence,

$$d\lambda = -\frac{1}{\nu^2}\, d\nu \tag{19}$$

One sometimes needs to use Eq. 19 in order to transform a wavenumber-dependent function into a wavelength-dependent function. For example, the black body radiant intensity as the function of wavenumber $I_{b\nu}$ is related to that as the function of wavelength $I_{b\lambda}$, such that

$$I_{b\nu}\, d\lambda = -I_{b\nu}\, d\lambda \ . \tag{20}$$

The minus sign is added for $I_{b\lambda}$ to be positive. From Eqs. 15, 19 and 20,

$$I_{b\lambda} = \frac{2hc^2}{\lambda^5} \frac{1}{e^{\frac{hc}{\lambda kT}} - 1} \ . \tag{21}$$

Also for other parameters, one can follow the above relationship. Sometimes, radiative parameters are expressed with respect ot the frequency of radiation. In this case, a similar relationship holds.

2. 4. 2. Radiant energy density

The radiant energy is equivalent to the energy of photons which passes through a control surface. Let us assume isotropic radiation. The radiative energy flux that passes through a unit area is

$$4\pi I_{\nu,isotropic} = u_\nu c \ , \tag{22}$$

where u_ν represents the radiant energy per unit volume and per unit wavenumber interval. It denotes 'spectral radiant energy density,' and is given by

$$u_\nu = \frac{4\pi I_{\nu,isotropic}}{c} \ . \tag{23}$$

2. 4. 3. Stefan-Boltzmann law

When the radiation is isotropic, that is, the radiant energy density is given by Eq. 23, the one-sided spectral radiant energy flux S_ν is

$$S_\nu = \frac{cu_\nu}{4} \ , \tag{24}$$

where c/4 is the mean velocity component in the direciton normal to the control surface. In radiative equilibrium, the total one-sided radiant energy flux is obained by integrating Eq. 24 with respect to wavenumber; Eq. 23 is substituted into u_ν. In turn, $I_{\nu,isotropic}$ in Eq. 23 is given by Eq. 15.

$$S_b = \int_0^\infty S_{b\nu} d\nu = \sigma T^4 \ . \tag{25}$$

Equation 25 is generally called 'Stefan-Boltzmann law.' The coefficient σ is 'Stefan-Boltzmann constant.'

$$\sigma = \frac{2\pi^5 k^4}{15 h^3 c^2} = 5.67 \times 10^{-8} \ [W/(m^2 K^4)] \ . \tag{26}$$

Equation 25 implies that in radiative equilibrium radiant energy flux depends only on the temperature of the medium.

2. 4. 4. Wall parameters

Figure 2.4 shows the schematics of radiant energy fluxes on a solid wall. Some fraction of the raidant energy flux incident on the wall is reflected. The other is absorbed by the wall. The ratio of the reflected energy flux to the total energy flux incident on the wall is called 'spectral reflectivity,' and is denoted by R_ν here. The ratio of the absorbed to the total energy flux is called 'spectral absorptivity,' and is denoted by A_ν here. Naturally,

$$A_\nu + R_\nu = 1 \tag{27}$$

The wall itself emits radiative energy by so-called thermal radiation. If the body is a blackbody, the radiant energy flux emitted from the wall is given by Eq. 25. Practically, a body is not necessarily black, but emits radiant energy flux smaller than that by a blackbody. In general, the radiant energy flux emitted from a wall is expressed by

$$S = e_w S_b \ . \tag{28}$$

Here, e_w is called the 'emissivity' of the wall, and ranges from zero to unity.

Both the reflectivity and emissivity of the wall depend strongly on the material of a body.

2. 4. 5. Gray medium approximation

In order to simplify a radiative transfer problem, 'gray medium' approximation is sometimes made. In this approximation, the absorption coefficient is assumed to be independent of wavenumber. Such approximation is useful in the case of radiative equilibrium in which an emission coefficient is related to an absorption coefficient by Kirchhoff's law.

However, absorption coefficient spectra of a high temperature gaseous medium, in general, depend strongly on the wavenumber. Hence, it is not applicable to such a nonequilibrium hypersonic shock layer as will be discussed in Chap. 5.

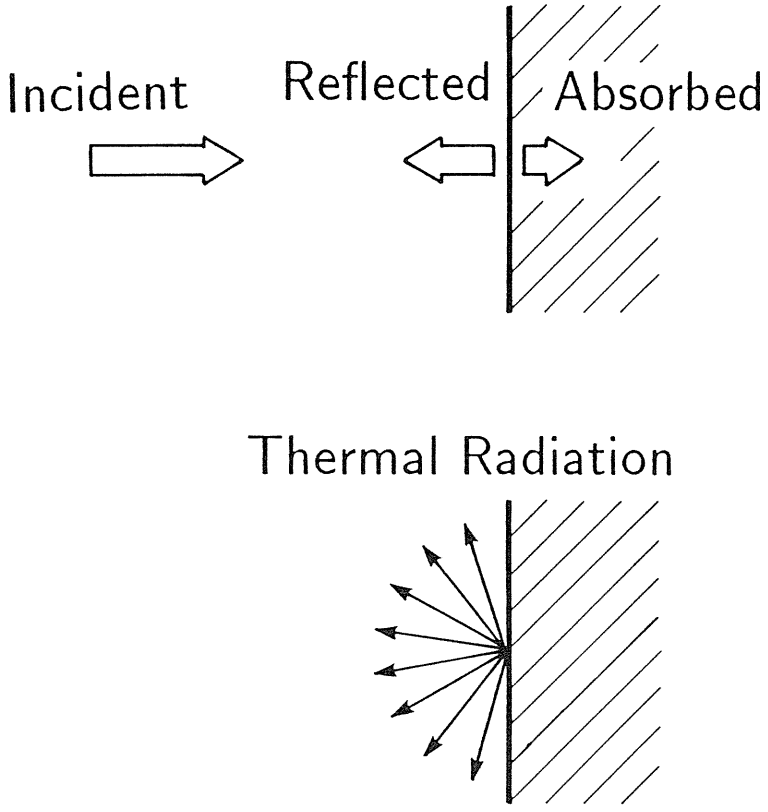

Fig. 2. 4. Radiative energy flux on wall.

3. Mechanisms of Radiative Emission and Absorption

3. 1. Atomic Spectra Calculation

3. 1. 1. Line spectra (bound-bound transition)

[Emission coefficient]

When an atom is at a high electronic level, other than its ground level, it has an internal energy, which is determined by its energy level diagram. Such an atom spontaneously emits a photon by the following process;

$$A(n') \rightarrow A(n'') + hc\nu_{n'n''}, \quad n' > n'' \tag{29}$$

Here $A(n')$ and $A(n'')$ represent atomic A-species at an upper and lower electronic levels, respectively. This process is called 'spontaneous emission.' Radiative energy emitted by the process is equal to the difference between the electronic energies at these levels.

$$hc\nu_{n'n''} = E(n') - E(n'') \equiv \Delta E_{n'n''} \tag{30}$$

One can find $\Delta E_{n'n''}$ for each electronic transition of an atom in literatures; e.g., the energy level diagrams of N and O are on p. 144 and p. 163 in Ref. 8), respectively.

Emission power $P_{n'n''}$ [W/m^3] is the product of $\Delta E_{n'n''}$, the probability of the transition $A_{n'n''}$ and the number density of the atom at an n'-level $N_{n'}$.

$$P_{n'n''} = 4\pi J_{n'n''} = N_{n'} A_{n'n''} \Delta E_{n'n''} \tag{31}$$

where $A_{n'n''}$ is called 'Einstein transition probability of spontaneous emission.' and has a unit of [s^{-1}]; it represents the frequency of the spontaneous emission by a single atom at n'-level provided that its electronic energy level goes back from n''- to n'-level immediately after a transition. $A_{n'n''}$ is related to a matrix element of transition $\mathbf{R}_{n'n''}$ by[7),5),14)]

$$A_{n'n''} = \frac{16\pi^3 \nu_{n'n''}^3}{3h\epsilon_0} \frac{1}{g_{n'}} \sum_{i,j} |\mathbf{R}_{n'_i n''_j}|^2 \tag{32}$$

Here, the subscripts i and j number the degenerate sublevels of the upper and lower states, respectively. In turn, $\sum|\mathbf{R}_{n'_i n''_j}|^2$ is expressed using an oscillator strength of emission $f_{emis,n'n''}$ by[5),14)]

$$|\mathbf{R}_{n'_i n''_j}|^2 = \frac{3e^2 h g_{n'} f_{emis,n'n''}}{8\pi^2 m_e c \nu_{n'n''}} \tag{33}$$

In order to calculate the emission power, one should know one of $A_{n'n''}$, $\sum|\mathbf{R}_{n'_i n''_j}|^2$ and $f_{emis,n'n''}$. These are found in such a literature as Ref. 9).

The emission coefficient j_ν is the radiative energy flux per unit solid angle and per unit wavenumber interval [$W/(m^2 \cdot m^{-1} \cdot sr)$]. It is related to Eq. 31, such that,

$$\begin{aligned} j_\nu &= J_{n'n''} L_e(\nu) \\ &= \frac{N_{n'} A_{n'n''} \Delta E_{n'n''}}{4\pi} L_e(\nu) \quad , \end{aligned} \tag{34}$$

where $L_e(\nu)$ is a line shape function[14)] which satisfies the followoing equation.

$$\int_0^\infty L_e(\nu) d\nu = 1 \quad . \tag{35}$$

[Absorption coefficient]

Integrated radiant intensity which is absorbed by atom gas of a physical thickness Δx along the ray $I_{abs,n'n''}$ [$W/(m^2 \cdot sr)$] is[7)]

$$I_{abs,n'n''} = \frac{1}{4\pi} u_{\nu,n'n''} N_{n''} B_{n''n'} hc\nu_{n'n''} \Delta x \tag{36}$$

Here, $u_{\nu,n'n''}$ $[J/(m^3 \cdot m^{-1})]$ is the spectral radiant energy density. $B_{n''n'}$ is the probability of absorption by an atom per unit spectral radiant energy density per unit time, and is called 'Einstein transition probability of absorption (Einstein's B-coefficient).' The unit of $B_{n''n'}$ depends on that of $u_{\nu,n'n''}$. Under the presnet definition, it is in the unit of $[m^3 \cdot m^{-1}/(J \cdot s)]$; $u_{\nu,n'n''}B_{n''n'}[s^{-1}]$ is the probability of a transition from n''- to n'-level. Since the spectral radiant intensity incident on the medium, $I^0_{\nu,n'n''}$, is equals to $u_{\nu,n'n''}c/(4\pi)$, Eq. 36 becomes

$$I_{abs,n'n''} = I^0_{\nu,n'n''} N_{n''} B_{n''n'} h\nu_{n'n''} \Delta x \tag{37}$$

$B_{n''n'}$ is related to the matrix moment of transition and to the oscillator strength of absorption, such that,[7),5),14)]

$$B_{n''n'} = \frac{2\pi^2}{3h^2 c\epsilon_0} \frac{1}{g_{n''}} \sum_{i,j} |\mathbf{R}_{n'_i n''_j}|^2 \tag{38}$$

$$|\mathbf{R}_{n'_i n''_j}|^2 = \frac{3e^2 h g_{n''} f_{abs,n''n'}}{8\pi^2 m_e c \nu_{n'n''}} \tag{39}$$

Using Eqs. 32 and 38, $B_{n''n'}$ is connected with $A_{n'n''}$.

$$\frac{A_{n'n''}}{B_{n''n'}} = 8\pi hc\nu^3_{n'n''} \frac{g_{n''}}{g_{n'}} \ . \tag{40}$$

From Eq. 37 and the relation;

$$I_{abs,n'n''} = \int_0^\infty (I^0_\nu - I_\nu) d\nu = I^0_{\nu,n'n''} \Delta x \int_0^\infty \kappa_\nu d\nu \ , \tag{41}$$

In the above equation, $I^0_{\nu,n'n''}$ is assumed constant over the width of the line. From Eqs. 37 and 41, the absorption coefficient $\kappa_\nu[m^{-1}]$ is given by

$$\int_0^\infty \kappa_\nu d\nu = N_{n''} B_{n''n'} h\nu_{n'n''} \ , \tag{42}$$

or

$$\kappa_\nu = N_{n''} B_{n''n'} h\nu_{n'n''} L_a(\nu) \ . \tag{43}$$

where $L_a(\nu)$ is a line shape function for absorption, and satisfies

$$\int_0^\infty L_a(\nu) d\nu = 1 \ . \tag{44}$$

[Line broadening]

Due to some broadening mechanisms, an atomic line spectrum does not vary like a delta function, but has a finite width. The line width is usually expressed with respect to wave-

length. The line broadening mechanisms are subdivided into the followings:

[1] Natural broadening; which is due to the uncertainty principle. The width at half-height is independent of wavelength,[15]

$$\Delta\lambda_{natural} = \frac{e^2}{3\epsilon_0 m_e c^2} = 1.18 \times 10^{-14}\ [m]\ . \tag{45}$$

[2] Doppler broadening; which is due to the thermal motion of radiating particles. The width at half-height is[14]

$$\Delta\lambda_{Doppler} = 2\left(\frac{2kTln2}{m_A c^2}\right)^{\frac{1}{2}}\lambda_{CL}\ . \tag{46}$$

[3] Pressure broadening; which is still more subdivided into [3-1] Stark broadening, [3-2] Resonance broadening and [3-1] Van der Waals broadening.

[3-1] is due to perturbation by charged particles. [3-2] and [3-3] are due to perturbation by neutral particles. The data of the line widths of [3-1] are listed in Ref. 14). From the data, the following approximation can be made.

$$\Delta\lambda_{Stark} = \Delta\lambda^{\circ}\left(\frac{T_e}{10^4}\right)^{l}\frac{N}{10^{22}}\ . \tag{47}$$

Here, $\Delta\lambda^{\circ}$ denotes the width at half-height under the condition that T_e=10^4 K and N=$10^{22}m^{-3}$, which is given in the literature.[14] The exponent l is obtained by data fitting.

The interaction between radiating neutral atoms and atoms of the same kind results in broadening of [3-2]. The line width due to [3-2] is calculated by[14]

$$\Delta\lambda_{resonance} = \frac{3}{32\pi^3 c}\left(\frac{g_{n'}}{g_{n''}}\right)^{1/2}\lambda^5 A_{n'n''}N\ , \tag{48}$$

The interactions between radiating neutral atoms and atoms of other kinds result in broadening of [3-3]. Some approximations are made in order to calculate the van der Waals line width. The details are found in such literatures as Refs. 14),15),19),20) and 11).

Among the above broadening mechanisms, [1] and [3] obey 'Lorentzian' profile. Approximately, these widths can be superimposed on each other, thereby yielding a Lorentzian width w_l.

$$w_l = \Delta\lambda_{natural} + \Delta\lambda_{Stark} + \Delta\lambda_{resonance} + \Delta\lambda_{van\ der\ Waals}\ . \tag{49}$$

The rest, i.e. Doppler broadening, obeys 'Gaussian' profile.

$$w_g = \Delta\lambda_{Doppler}\ . \tag{50}$$

Here, the line shape is assumed to obey 'Voigt profile,' given by[10]

$$j_\lambda = j_{\lambda CL}\left[\left(1 - \frac{w_l}{w_v}\right) exp\left\{-2.772\left(\frac{\lambda - \lambda_{CL}}{w_v}\right)^2\right\} + \frac{w_l/w_v}{1 + 4\left\{(\lambda - \lambda_{CL})/w_v\right\}^2}\right.$$

$$+ 0.016\left(1 - \frac{w_l}{w_v}\right)\left(\frac{w_l}{w_v}\right)\left[exp\left\{-0.4\left(\frac{\lambda - \lambda_{CL}}{w_v}\right)^{2.25}\right\}\right.$$

$$\left.\left. - \frac{10}{10 + \left\{(\lambda - \lambda_{CL})/w_v\right\}^{2.25}}\right]\right] \tag{51}$$

$$j_{\lambda CL} = \frac{j_{n'n''}}{w_v\left[1.065 + 0.447(w_l/w_v) + 0.058(w_l/w_v)^2\right]} \ . \tag{52}$$

The Voigt line width is expressed using w_l and w_g.

$$w_v = \frac{w_l}{2} + \left[\left(\frac{w_l}{2}\right)^2 + w_g^2\right]^{\frac{1}{2}} \ . \tag{53}$$

3. 1. 2. Continuum 1 (bound-free transition)

One of the radiation mechanisms which results in continuum is bound-free transition of an atom.

$$A_{n'} + hc\nu \rightleftharpoons A^+ + e \tag{54}$$

Here, $A_{n'}$ denotes an atomic A-species at an n'-electronic energy level. The process in the forward direction is 'photoionization.' That in the reverse direction is radiative capture of an electron. From an elementary relation, the absorption coefficient due to photoionization is given by,[5),15)]

$$\kappa_\nu = \sigma_{p,\nu} N_{n'}\left[1 - exp\left(-\frac{hc\nu}{kT_e}\right)\right] \ . \tag{55}$$

The emission coefficient due to the radiative capture is

$$j_\nu d\nu = \frac{1}{4\pi} N_+ N_e f(\nu)\nu d\nu \sigma_c hc\nu \ . \tag{56}$$

Here, the energy of a photon is determined by the difference between the electronic plus electron-translational energies after and before the process.

$$hc\nu = \frac{1}{2} m_e v^2 + E_{ionization} - E_{n'} \ . \tag{57}$$

The data of the cross-sections and some approximations of the spectrum are given in literatures, e.g. Ref 15).

3. 1. 3. *Continuum 2 (free-free transition)*

Decelerating a free electron with some translational energy by the electric field generated by a charged particle results in radiative emission. This process is called 'bremsstrahlung,' and causes continuous spectra. The reverse process, i.e. the acceleration of a free electron with the absorption of a photon, is called 'inverse-bremsstrahlung.' The emission and absorption coefficients by these processes are given by Kramers.[15].

$$j_\nu = \frac{e^6}{12\pi^2 c^2 \epsilon_0^3 (6\pi m_e^3 k)^{1/2}} \frac{n_e n_+}{T_e^{1/2}} exp\left(-\frac{hc\nu}{kT_e}\right) , \tag{58}$$

$$\kappa_\nu = \frac{e^6}{24\pi^2 c^4 \epsilon_0^3 h (6\pi m_e^3 k)^{1/2}} \frac{n_e n_+}{\nu^3 T_e^{1/2}} exp\left(-\frac{hc\nu}{kT_e}\right) . \tag{59}$$

Under such a condition as is dealt with in Chapter 5, almost all the charged particles are singly ionized. Therefore, one can assume that $n_+=n_e$. It follows that the emission and absorption coefficients due to these processes scale with the square of elecron density.

3. 2. *Molecular Spectra Calculation*

3. 2. 1. *Radiative transition and band spectra*

The method of calculation of molecular spectra is similar to that of atomic line spectra. However, in the case of a molecule, an electronic transition is accompanied by a vibrational and rotational transitions.

A radiative transition of a molecule is, in general, expressed by

$$M(n',v',J') \rightarrow M(n'',v'',J'') + hc\nu_{n',v',J',n'',v'',J''} \tag{60}$$

Here, $M(n',v',J')$ represents a molecule at an n'-electronic, v'-vibrational and J'-rotational energy levels. Figure 3.1 shows the energy diagram of a molecule. At an electronic energy leve, vibrational energy levels lie at intervals which are much smaller than the electronic energy intervals. At each vibrational energy level, rotational energy levels lie at intervals which are much smaller than the vibrational energy intervals. Also in this figure, the respective energies at electronic B-level, $v'=2$ and $J'=8$ are shown.

The radiative energy emitted by the transition is the sum of the energy differences associated with the respective energy modes.

$$hc\nu_{n',v',J',n'',v'',J''} = \Delta E_{el} + \Delta E_{vib} + \Delta E_{rot} \tag{61}$$

Here, in many cases,

$$|\Delta E_{el}| >> |\Delta E_{vib}| >> |\Delta E_{rot}| .$$

The radiation which corresponds to the energy given by Eq. 61 lies mainly in the ultraviolet and visible ranges.

Figure 3.2 shows the example of the potential curves of a diatomic molecule. The ordinate represents the internal energy of the molecule. The abscissa represents the internuclear distance. The curves which enclose horizontal lines are the trace of vibrational motion at an

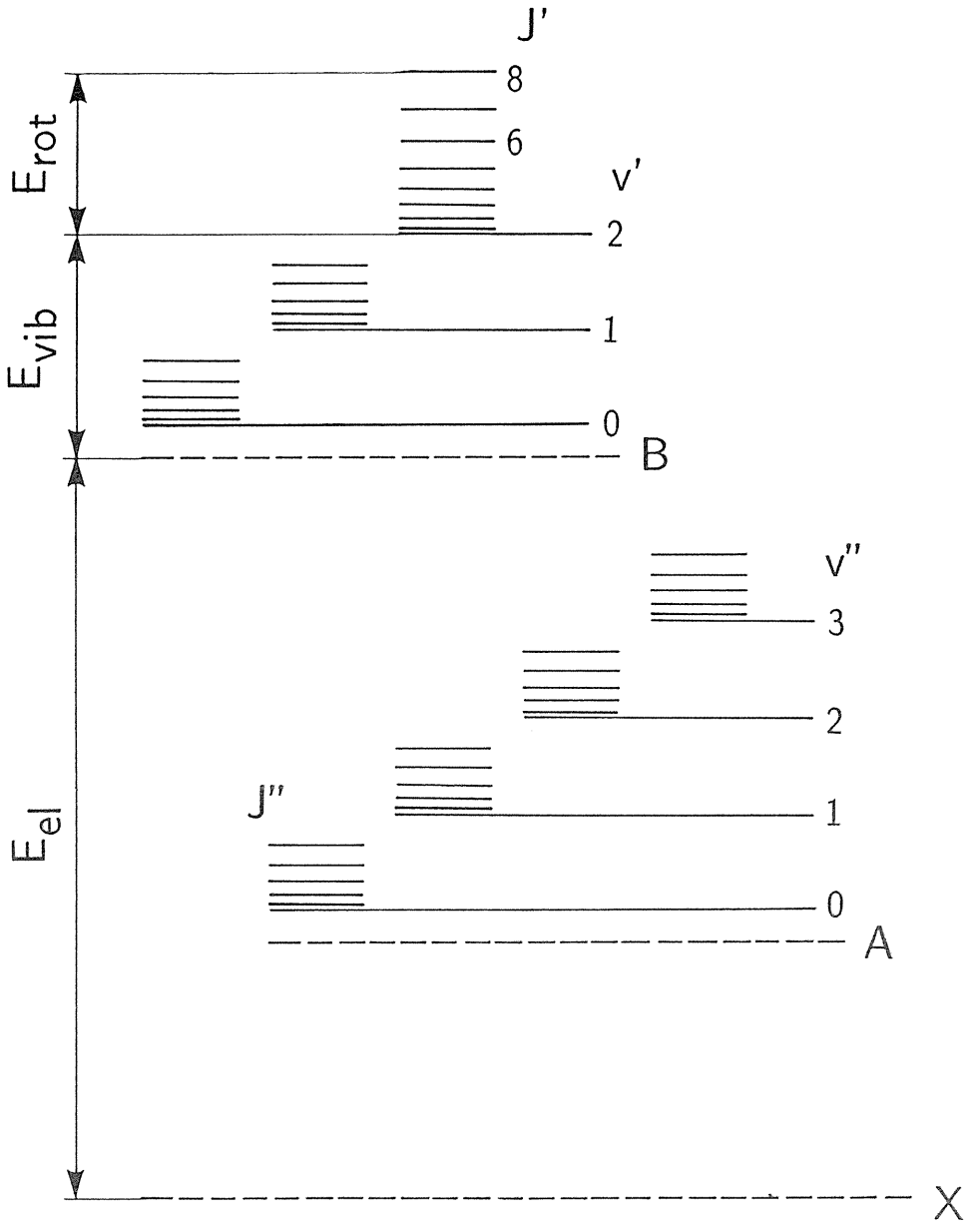

Fig. 3. 1. Schemdatics of energy diagram of diatomic molecule.

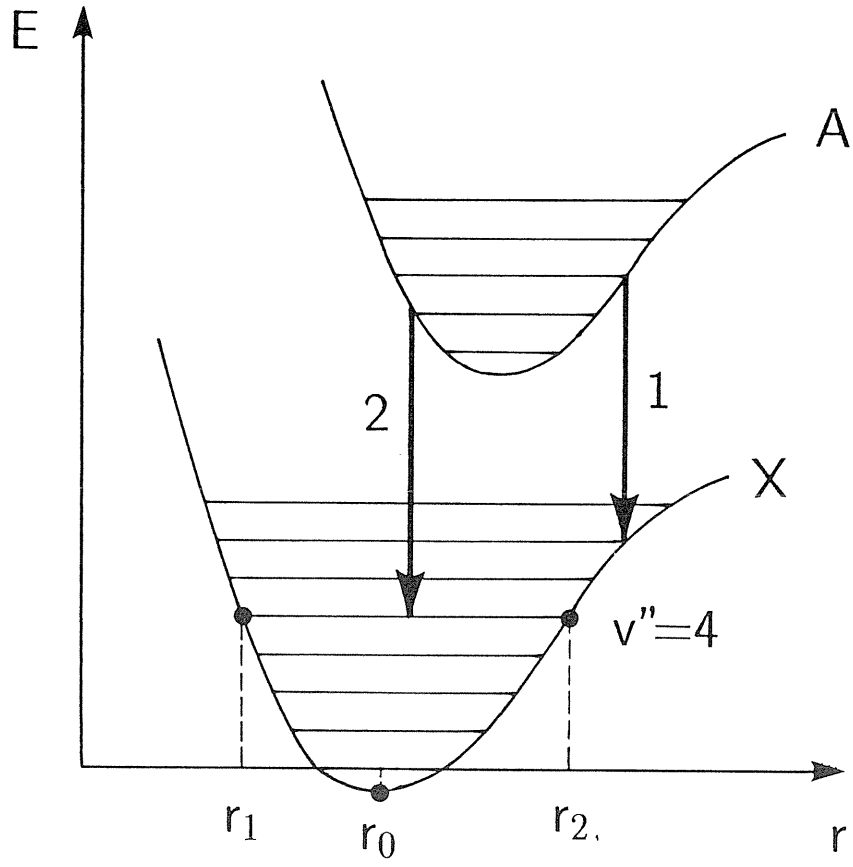

Fig. 3. 2. Potential curves for diatomic molecule.

electronic-vibrational energy level. The enclosed lines represent vibrational energy levels. For example, when the molecule is at an electronic X-level, and at a vibrational quantum number $v''=4$, the two nuclei vibrate along the curve between points $r=r_1$ and $r=r_2$. A repulsive force is exerted on the nuclei at $r=r_1$ to r_0. An attractive force does at $r=r_0$ to r_2.

Transitions with radiative emission is expressed by the arrows drawn in the vertically downward direction in Fig. 3.2. Since an electronic transition occurs for a sufficiently short time, one can neglect the vibrational motion during the transition. Although, as will be described later, there are some conditions under which a transition is able to occur, or occurs at a high probability, a transition occurs in such a way that the internuclear distance remains almost constant during the transition.

On a vibrational transition, there is not such a strick selection rules as on a rotational transition which will be described later. Instead, on the probability of the transition, 'Franck-Condon principle' is applied. This principle is based on the fact that the vibrational quantum number after a transition depends on the correlation of eigenfunctions at the upper and lower

levels.[7] A vibrating nucleus reside for a long time in the vicinity of the turning points, e.g. $r=r_1$ and $r=r_2$ in Fig. 3.2. This holds both for the upper and for lower levels of transition. Therefore, transition 1 occurs at a probability much higher than that of transition 2.

On the change in rotational quantum number during a transition, there exists general selection rules:

$$\Delta J = 0, \pm 1$$

with the restriction that a transition $J=0$ to $J=0$ is forbidden.

Although the above selection rule generally holds for electric dipole radiation, there exist some other selection rules, which are given in literatures.[7]

3. 2. 2. Term symbols on molecular electronic level[7]

The electronic level of a molecule is designated by X,A,B, · , · , · , a,b, · , · , · . Usually, a ground state is designated by X.

The absolute value of the component of the electronic orbital angular momentum about the internuclear axis is denoted by Λ. The corresponding term symbols according as $\Lambda=1,2,3,4, \cdots$ are $\Sigma,\Pi,\Delta,\Phi, \cdots$.

The quantum number of the resultant of electron spins is denoted by S. S is integer or half-integer according as the total number of electrons is even or odd. In the internuclear direction, it has a component Σ, which can range such as

$$\Sigma = S, S-1, \cdots, -S ,$$

implying that there are $2S+1$ different values of Σ. If $S \neq 0$, the electronic energy slightly splits into $2S+1$ levels. Therefore, $2S+1$ is called 'multiplicity,'

In order to express a molecular electronic state, the above designation are combined, such as,

$$^{2S+1}\sum_{\Lambda+\Sigma} ,$$

where the large Σ implies that $\Lambda=0$, and is replaced by $\Pi,\Delta,\Phi, \cdots$ according as $\Lambda=2,3,4, \cdots$. The subscript, which is not always added, represents the quantum number component of the resultant of the electron spins and the electronic orbital augular momenta, i.e. the total electronic angular momenta, in the internuclear direction.

Any plane which passes through both nuclei is a plane of symmetry. On one hand, if the eigenfunction does not change the sign when reflected with respect to the plane, a superscript '+' is used. If, on the other hand, the sign is changed, a superscript '−' is used.

If the two nuclei have the same charge, the point on the internuclear axis at the same distance from the nuclei becomes a center of symmetry. If the sign of the eigenfunction is unchanged by the reflection with respect to the center of symmetry, a subscript 'g' (from 'gerade' in German) is used. If the sign is changed, a subscript 'u' (from 'ungerade') is used.

For example, the lower level of N_2 first positive band is $A^3\Sigma_u^+$. The quantum number of the electronic orbital angular momentum $\Lambda=0$. The quantum number of electron spin $S=1$ ($2S+1=3$; triplet). The sign of the eigenfunction is unchanged by the reflection with respect to the surface which goes through both nuclei. The sign is changed by the reflection with respect to the center of symmetry.

3. 2. 3. Molecular internal energies

Here, a vibrating rotator model[7] is assumed. Neglecting the coupling of the rotational and electronic motions, but taking the couling of the rotational and vibrational motions into account, the rotational energy of a molecule at a rotational quantum number J is given by

$$F(J) = B_v J(J+1) - D_v J^2 (J+1)^2 \tag{62}$$

Here, $F(J)$ is in the unit of wavenumber $[m^{-1}]$. In Eq. 62, the effect of the centrifugal force of the rotating molecule is included in the second term of the right-hand side and in the correction for B_v. The quantities B_v and D_v depend on the electronic energy level and on the vibrational quantum number. To first approximation, these are expressed, as follows,[7]

$$B_v = B_e - \alpha_e (v + \frac{1}{2}) \tag{63}$$

where B_e is the rotational constant of a rigid rotator.

$$B_e = \frac{h}{8\pi^2 cI} \tag{64}$$

The second term of the right-hand side in Eq. 63 is due to change in the internuclear distance. Since the change in the internuclear distance is much smaller than the distance itself, the ratio α_e / B_e is usually much smaller than unity.

In the same manner, another rotational constant D_v is approximately given by

$$D_v = D_e + \beta_e (v + \frac{1}{2}) \ . \tag{65}$$

$$D_e = \frac{4B_e^3}{\omega_e^3} \ . \tag{66}$$

Here, ω_e is the wavenumber of the molecular vibration. Also, the ratio β_e / D_e is usually much smaller than unity.

Using the above equations, the difference in rotational energy is given by

$$\Delta E_{rot} = hc[F(J') - F(J'')] \ . \tag{67}$$

The vibrational energy is a function of a vibrational quantum number, and is usually approximated by[7]

$$G(v) = \omega_e (v + \frac{1}{2}) - \omega_e x_e (v + \frac{1}{2})^2 + \omega_e y_e (v + \frac{1}{2})^3 + \omega_e z_e (v + \frac{1}{2})^4 \ . \tag{68}$$

The vibrational energy difference is

$$\Delta E_{vib} = hc[G(v') - G(v'')] \ . \tag{69}$$

The electronic energy difference is obtained from the electronic energies of the upper and lower electronic states at their vibrational and rotational ground levels.

$$\Delta E_{el} = hc[T_{el}(n') - T_{el}(n'')] \tag{70}$$

The values of T_{el} are found in the energy level diagram of a molecule.

In calculating the energy differences of existing molecular spectra, some modification is necessary. The details are described in Refs. 7) and 10). In this study, the effect of the coupling of molecular rotation and electronic motion is taken into account in some cases. This needs modifications of the expression of molecular rotational energy, which are described in Appendix.

3. 2. 4. Integrated intensity and broadening of spectra

The integrated emission coefficient due to a single electronic-vibrational-rotational transition is given by,[7),10)]

$$J_{n',v',J',n'',v'',J''} = \frac{4\pi^2 cN_u \tilde{\nu}^4}{3\epsilon_0(2J'+1)} |R_e(\bar{r}_{v'v''})|^2_{av} q_{v'v''} S^{J'\Lambda'}_{J''\Lambda''} \ . \tag{71}$$

In the above equation, N_u denotes the number density of the molecules at the upper state. $|R_e(\bar{r}_{v'v''})|^2_{av}$ is the average of the square of the electronic transition moment, and is obtained by

$$|R_e(\bar{r}_{v'v''})|^2_{av} = \frac{1}{g_{v'}} \sum_{i,j} |R_e(\bar{r}_{v'_i v''_j})|^2 \ , \tag{72}$$

which, in turn, is related to the absorption f-number by

$$\sum_{i,j} |R_e(\bar{r}_{v'_i v''_j})|^2 = \frac{3he^2 hg_{v''} f_{abs}(\nu)}{8\pi^2 m_e c \nu_{v'v''}} \tag{73}$$

The value of the f-number, which is a function of wavenumber, is obtained from literatures.[16)] The Franck-Condon factor $q_{v'v''}$ and the line strength factor $S^{J'\Lambda'}_{J''\Lambda''}$ are obtained from theory.[10)]

The line shape of a molecule, as does atomic spectra, obeys the Voigt profile (Eq. 51). In this case, the Lorentzian width at half-height is given by[11)]

$$w_l = \Delta\lambda_{natural} + \Delta\lambda_{Stark} + \Delta\lambda_{col,1} + \Delta\lambda_{col,2} \ . \tag{74}$$

Here, $\Delta\lambda_{col,1}$ denotes the line width due to the broadening by the colisions with a like molecule. $\Delta\lambda_{col,2}$ does that by the collisions with all other molecules. The line width due to collision broadening is obtained by Lorentz.[17),18)]

$$\Delta\lambda_{col} = 6.74 \times 10^{10} \frac{\lambda^2_{CL}}{c} \sigma_1\sigma_2 \left(\frac{1}{M_1} + \frac{1}{M_2}\right)^{1/2} \frac{p}{T^{1/2}} \ , \tag{75}$$

where collision diameters σ_1 and σ_2 are in angstroms, molecular weights M_1 and M_2 in [g/mol], pressure p in [atom], T in [K], $\Delta\lambda_{col}$ and λ_{CL} in [m] and c in [m/s], respectively.

3. 3. *Determination of Number Densities*

3. 3. 1. *Thermal equilibrium case*

In calculating the emission and absorption coefficients by atoms or molecules, one should know the number density of the species at the energy level from which the transition takes place. If the molecular gas is in thermal equilibrium with respect to the respective internal modes, the nubmer density is calculated using partition functions.

$$N_A(n,v,J) = N_A \frac{Q(n,v,J)}{Q} \quad . \tag{76}$$

The partition function of a molecule at an (n,v,J) energy level and the associated with the whole energy levels are respectively given by[10]

$$Q(n,v,J) = g(n)\,(2J+1)\,exp[-\frac{hc}{k}\{\frac{T_{el}(n)}{T_{el}} + \frac{G(v)}{T_{vib}} + \frac{F(J)}{T_{rot}}\}] \quad , \tag{77}$$

$$Q = \sum_{n=1}^{n_{max}} [g(n)exp(-\frac{hcT_{el}(n)}{kT_e}) [\sum_{v=0}^{v_{max}} \frac{kT_{rot}}{hcB_v(v)} exp\{-\frac{hcG(v)}{kT_{vib}}\}]] \quad , \tag{78}$$

in which T_e, T_{vib} and T_{rot} denote the electronic, vibrational and rotational temperatures, respectively.

In the case of an atom, a similar calculation should be carried out. However, in this case, the transition is accompanied neither by a vibrational nor rotational one, resulting in a simpler formulation than that in the case of a molecule.

3. 3. 2. *Electronical nonequilibrium case*

If the energy relaxation characteristic times among internal modes are comparable with or longer than the flow resident characteristic time, Eq. 76 does not give a actual distribution of the number density. Under a reentry condition, for example, such situation can occur, in particular, on the electronic mode. In this case, the numer density of molecules at each electronic energy level is to be calculated by accounting for the rates of all possible elementary processes:

1) Electron impact ionization

$$M(n',v',J') + e \rightleftharpoons M^+(n'',v'',J'') + e + e \tag{79}$$

2) Electron impact excitation

$$M(n',v',J') + e \rightleftharpoons M(n'',v'',J'') + e \tag{80}$$

3) Heavy-particle impact ionization

$$M(n',v',J') + M' \rightleftharpoons M^+(n'',v'',J'') + M' + e \tag{81}$$

4) Heavy-particle impact excitation

$$M(n',v',J') + M' \rightleftharpoons M(n'',v'',J'') + M' \tag{82}$$

5) Radiative bound-bound transition

$$M(n',v',J') \rightleftharpoons M(n'',v'',J'') + hc\nu_{n'v'J',n''v''J''} \tag{83}$$

6) Radiative bound-free transition

$$M(n',v',J') + hc\nu \rightleftharpoons M^{+}(n'',v'',J'') + e \tag{84}$$

In order to determine the number densities, one should take only dominant processes into account instead of considering the principle of detailed balancing in all the above elementary processes. Under such a condition as is dealt with in Chap. 5, the processes 1), 2) and 5) dominate over the others in determining the nubmer densities.[12] The detailed balancings in the processes 1) and 2) result in so-called 'Saha equilibrium' or 'local thermodynamic equilibrium (LTE).' Such situation occurs when the density level of the gas is sufficiently high. In contrast, at a low density level, the density of molecules at each energy level is determined by the detailed balancing of the porcess 5), which results in 'coronal equilibrium.'

In order to calculate the nubmer densities at an intermediate density level, a 'quasi-steady state'[12),13)] condition associated with n'-level is assumed.

$$\sum_{n''} (K_{A,n''n'} n_e + A_{A,n''n'}) n_{A,n''} - \sum_{n''} (K_{A,n'n''} n_e + A_{A,n'n''}) n_{A,n'} = 0 \tag{85}$$

Here, $K_{A,n''n'}$ and $A_{A,n''n'}$ denote the rates of process 2) and 5), respectively. Eq. 85 establishes a set of linear equations, whose solutions are the nubmer densities at the respective energy levels. Detailed descriptions on this subject are found in Refs. 12) and 13).

As will be shown in Sec. 3.4, in order to calculate the radiation of N_2 second-positive band and that of O_2 Shumann-Runge band, it is necessary to calculate the number densities of $N_2C^3\Pi_u$ and $O_2B^3\Sigma_u^-$, respectively. However, these energy levels are above the respective dissociation limits. In these cases, the following balancing is assumed.[12]

$$M(n') + M(n'') \rightleftharpoons M_2(m') \rightharpoonup M_2(m'') + hc\nu \tag{86}$$

The left-harpoon represents predissociation.[7] The inverse-predissociation is represented by the first right-harpoon. The second right-harpoon does radiative transition into a lower energy level of the molecule M_2. Now, let the rates of the predissociation and inverse-dissociation be denoted by k_p and k_{ip}, respecively. The balancing in Eq. 86 is expressed by

$$k_{ip} n_{M(n')} n_{M(n'')} = (k_p + A_{m'm''}) n_{M_2(m')} \tag{87}$$

$$n_{M_2(m')} = \frac{k_p}{k_p + A_{m'm''}} n_E \tag{88}$$

$$n_E = \frac{k_{ip}}{k_p} n_{M(n')} n_{M(n'')} \tag{89}$$

3. 4. Spectra of Air

The air spectra calculated in this study are tabulated in Table 3.1. For atomic species, spectra by bound-bound, bound-free and free-free (bremsstrahlung and inverse-bremsstrahlung) transitions are taken into account. In addition, as shown in the table, six molecular band spectra are calculated.

Table 3. 1. Air spectra calculated in this study.

species		band name	transition
atom	N		bound ↔ bound, bound ↔ free
	N^+		free ↔ free
	O		bound ↔ bound, bound ↔ free
	O^+		free ↔ free
molecule	N_2^+	first negative	$B\,^2\Sigma^+_u \leftrightarrow X\,^2\Sigma^+_g$
	N_2	first positive	$B\,^3\Pi_g \leftrightarrow A\,^3\Sigma^+_u$
		second positive	$C\,^3\Pi_u \leftrightarrow B\,^3\Pi_g$
	NO	β system	$B\,^2\Pi \leftrightarrow X\,^2\Pi$
		γ system	$A\,^2\Sigma^+ \leftrightarrow X\,^2\Pi$
	O_2	Schumann-Rung	$B\,^3\Sigma^-_u \leftrightarrow X\,^3\Sigma^-_g$

4. Numerical Technique of Radiative Transfer Calculation: Band Method with Series-Expansion Approximation

4. 1. Smoothing of Radiant Intensity

In Eq. 9, the radiant intensity I_ν is a function of the wave number ν, and the direction of the ray ω. Since the amount of the spectral data of the emission and absorption coefficients is too much to perform direct spectral calculation, the wavenumber range of the calculation is subdivided into finite bands; the j-th band ranges from $\nu_{l,j}$ to $\nu_{u,j}$. For a volume element in which emission and absorption coefficients are spatially uniform, integration of Eq. 9 with respect to the wave number yields

$$I_{sm,j}(L)\Delta\nu_j = \int_{\nu_{l,j}}^{\nu_{u,j}} (1 - e^{-\kappa_\nu L}) \frac{j_\nu}{\kappa_\nu} d\nu + I_{sm,j}(0) \int_{\nu_{l,j}}^{\nu_{u,j}} e^{-\kappa_\nu L} d\nu \ . \tag{90}$$

In the above equation, L is the transmitting distance of the ray though the volume element, and $I_{sm,j}(\omega)$ is a smoothed radiant intensity of the band (Fig. 4.1), and given by

$$I_{sm,j}(\omega) = \frac{1}{\Delta\nu_j} \int_{\nu_{l,j}}^{\nu_{u,j}} I_\nu(\omega) d\nu \ . \tag{91}$$

Here, ω denotes a coordinate set on a light ray.

For an optically thin element ($\kappa_\nu L << 1$),

$$e^{-\kappa_\nu L} = \sum_{k=0}^{\infty} \frac{(-1)^k}{k!} (\kappa_\nu L)^k \tag{92}$$

Hence, Eq. 90 is approximated by the following equation:[22)]

$$I_{sm,j}(L)\Delta\nu_j = I_{sm,j}(0)\Delta\nu_j + \sum_{k=1}^{N} [a_{k,j} I_{sm,j}(0) + b_{k,j}] L^k \ . \tag{93}$$

Here,

$$a_{k,j} = \frac{(-1)^k}{k!} \int_{\nu_{l,j}}^{\nu_{u,j}} \kappa_\nu^k d\nu \ . \tag{94}$$

$$b_{k,j} = -\frac{(-1)^k}{k!} \int_{\nu_{l,j}}^{\nu_{u,j}} \kappa_\nu^{k-1} j_\nu d\nu \ . \tag{95}$$

In order to calculate the smoothed radiant intensity after passing through an element $I_{sm,j}(L)$ from that incident on the element $I_{sm,j}(0)$, $a_{k,j}$ and $b_{k,j}$ are needed to be calculated from the spectral data of emission and absorption coefficients, which are calculated in such a way as is described in Chapter 3. Then, the coefficients $a_{k,j}$ and $b_{k,j}$ are to be memorized as substitutes for the spectral emission and absorption coefficients, thereby decreasing the requirement of the memory size for the radiative transfer calculation. On one hand, for example, the whole of the spectral data at a point in this study amounts to $2\times N_{array}$=40000. On the other hand, sufficiently accurate results are obtained by the present method with N_{ex}=2 and N_{band}=500; the number of the coefficients given by Eqs. 94 and 95 is $2\times N_{ex}\times N_{band}$=2000 — just one-twentieth of that of the spectral data.

4. 2. Radiative Heat Transfer to Wall

The radiative heat flux to the wall is obtained by integrating the radiant intensity with respect both to the solid angle 2π and to the wavenumber.

$$q_r = \int_0^\infty \int_{(2\pi)} I_{\nu,w} \cdot \mathbf{n}_n d\omega d\nu \tag{96}$$

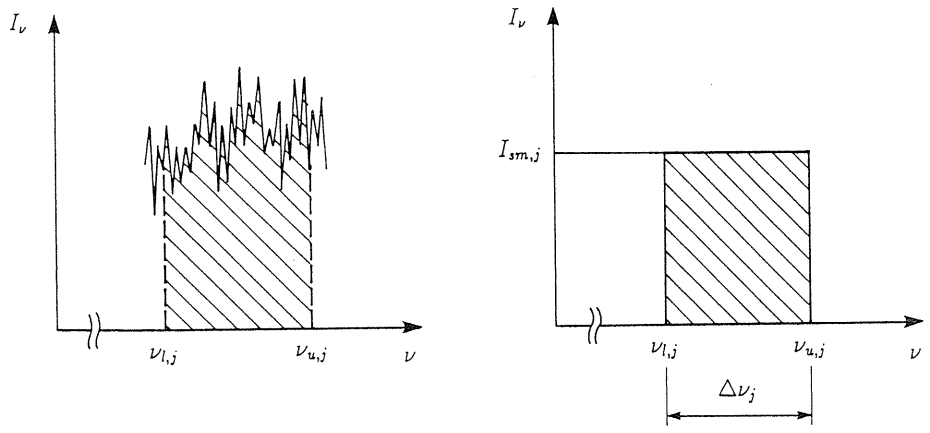

Fig. 4. 1. Smoothing of radiant intensity.

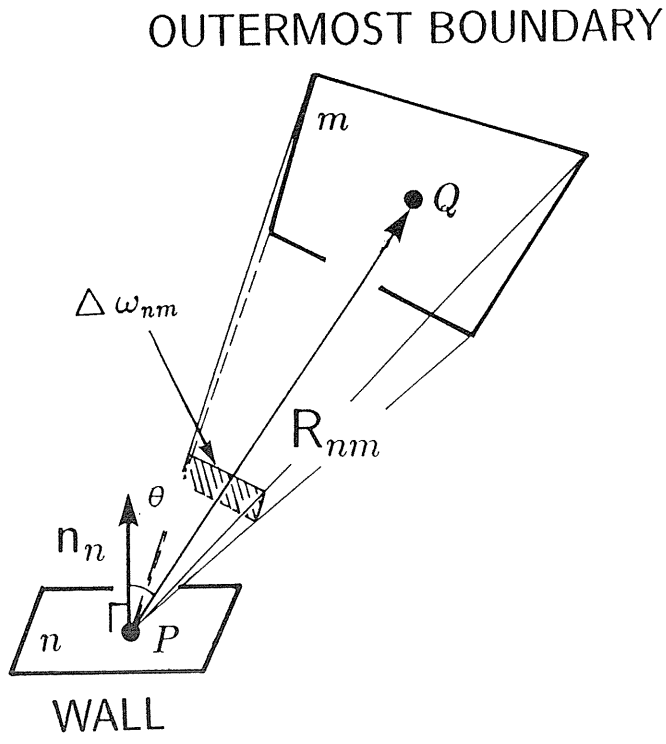

Fig. 4. 2. Radiative heat flux at a point on wall.

Here, $I_{\nu,w}$ denotes a radiant intensity on the wall, which is obtained by solving the radiative transfer equation. In this study, smoothed radiant intensity on the wall is calculated by the tracing of a light ray form the outermost boundary of the calculated domain to the wall. To each volume element through which the light ray goes, Eq. 93 is applied.

A convex body makes the ray tracing vastly simple. In Fig. 4.2, for a point visible from point P,

$$\mathbf{n}_n \cdot \mathbf{R}_{nm} > 0 \ . \tag{97}$$

The integral with respect to the solid angle in Eq. 96 is converted to the surface integral with respect to the outermost boundary of the calculated domain.

$$q_{r,n} = \sum_{j}^{j_{max}} \sum_{m,\mathbf{n}\cdot\mathbf{R}_{nm}>0} I_{sm,j,nm} \Delta \nu_j \frac{(\mathbf{n}_n \cdot \mathbf{R}_{nm}) \Delta \omega_{nm}}{|R_{nm}|} \tag{98}$$

In Eq. 98, $I_{sm,j,nm}$ is calculated by applying Eq. 93 along the ray under the condition that $I_{sm,j}=0$ at the outermost boundary.

If a body has concave parts, however, integral with respect to the solid angle is converted into surface intergral with respect not only to the outermost boundary but also to the body surface itself visible from the point. Hence, some modification of the ray tracing is necessary for such a body.

4. 3. Comparison with Edwards' Band Method

On radiative transfer problem, the band method by Edwards[23] is well known. On one hand, his method is for infrared spectra which is caused by vibrational-rotational trnasitions of molecules. On the other hand, the present method deals with spectra due to electronic transition of atoms and electronic-vibrational-rotational transitions of molecules. Moreover, these two method are essentially different as follows:

1) In Edwards' method, the smoothing of radiant intensity is conducted for each band system. Hence, the 'block calculation'[23] is needed in order to calculate the effective transmissivity. In contrast to this, in the present method, the smoothing is done after superimposing all the emission and absorption coefficients made by all the species, respectively. Therefore, one does not need to conduct the block calculation.

2) In Edwards' method, the band absorption is given according to the exponential-tailed band model, implying that there is a limitation on the spectrum shape (wavenumber dependence of band) for his method to be applied. However, the condition of the application of the present method is only that a volume element must be optically thin, i.e., $\kappa_\nu L << 1$ in the whole wavelength range. There is no limitation on the wavenumber-dependence of the spectrum.

3) Edwards' method assumes local radiative equilibrium, i.e., that the Kirchhoff's law holds in the calculation domain. However, the present method deals with a medium in raidative nonequilibrium; the emission coefficient is not necessarily related to the absorption coefficient using a blackbody intensity.

5. Application; Radiative Field around a Hypersonic Blunt Body

5. 1. *Flow-Chart of Calculation*

The problem of radiative heat transfer from hypersonic shock layers becomes important in designing a reentry vehicle; it has been pointed out that the radiative heat transfer can be comparable with or larger than the convective one.[2),3),4)] A condition of reentry, e.g., is an altitude of 70 km and a flight Mach number of 35 (a flight velocity of 10 km/s) or higher. In this case, thermal equilibrium does not hold, in particular, immediately behind the shock wave; the temperature which corresponds to an internal mode is not necessarily equal to that to another internal or translational mode. Furthermore, since the stagnation temperature is at high levels, chemical reactions including dissociations and ionizations take place in the shock layer. The characteristic times of the chemical reactions can be comparable with the flow resident time. Hence, the source term in the conservation equations must be calculated using finite rates of the foward and backward reactions. Simply saying, the shock layer is also in chemical nonequilibrium.

In order to calculate the radiative field in such a hypersonic shock layer, one needs to obtain the solution of the flowfield around a body. As mentioned above, such a flowfield contains both chemically and thermally nonequilibrium aspects. Figure 5.1 shows the flowchart of the radiative transfer calculation. In this study, the flowfield without heat input due to the emission and absorption of radiation is calculated (step 1).[24)-27)] Using the calculated flow properties, i.e., the temperatures and the number densities of the respective species, emission and absorption coefficients are calculated by the method shown in Sec. 3 (step 2); the NEQAIR program made by Park[11),12)] was used. In turn, these coefficients are input into radiative transfer calculation code (see Chap. 4), obtaining the radiative heat transfer over the wall (step 3).

From the emission coefficients calculated at step 2, the heat input by the radiation can be calculated. Basically, it is to be fed back to the flowfield calculation (step 1). However, as will be shown in Sec. 5.6, without the effect of radiative emission on the energy conservation of the flowfield, sufficiently accurate solutions are obtained.

Here, typical eleven air species, N, O, N_2, O_2, NO, N^+, O^+, N_2^+, O_2^+, NO^+ and e, are assumed to exist. Thermally nonequilibrium condition is taken into account by employing Park's two-temperature model.[13),28)] In this model, the heavy-particle translational and rotational temperatures are assumed to be the same and are denoted by T, and the vibrational and electron translational temperatures are assumed to be the same and are denoted by T_{ve} here. From the rates of 17 elementary reactions,[27)] the source terms in the fluid equations are calculated. The rates depend both on T and on T_{ve} independently.[28)] On the relaxation of vibrational energy, Landau-Teller type relaxation is assumed. The characteristic time is the sun of that by Millikan and White[29)] and the correction term by Park.[13)] Transport coefficients, i.e., thermal conductivity, viscosity and diffusion coefficient are given by Yoe's formulation.[30),31)]

5. 2. *Flowfield Condition*

Figure 5.2 shows the blunt body used as the model of the presnet calculation. The body is composed of a spherical part of 1 m in radius and a conical part with a half angle of 20 degrees. The upstream flow is assumed to be uniform and be parallel with the center axis (no angle of attack). The x-axis lies along the center axis. The origin is located at the stagnation point on the wall. The y-axis originates at the same point and goes along the wall. The gridding was made by a shock-fitting technique.

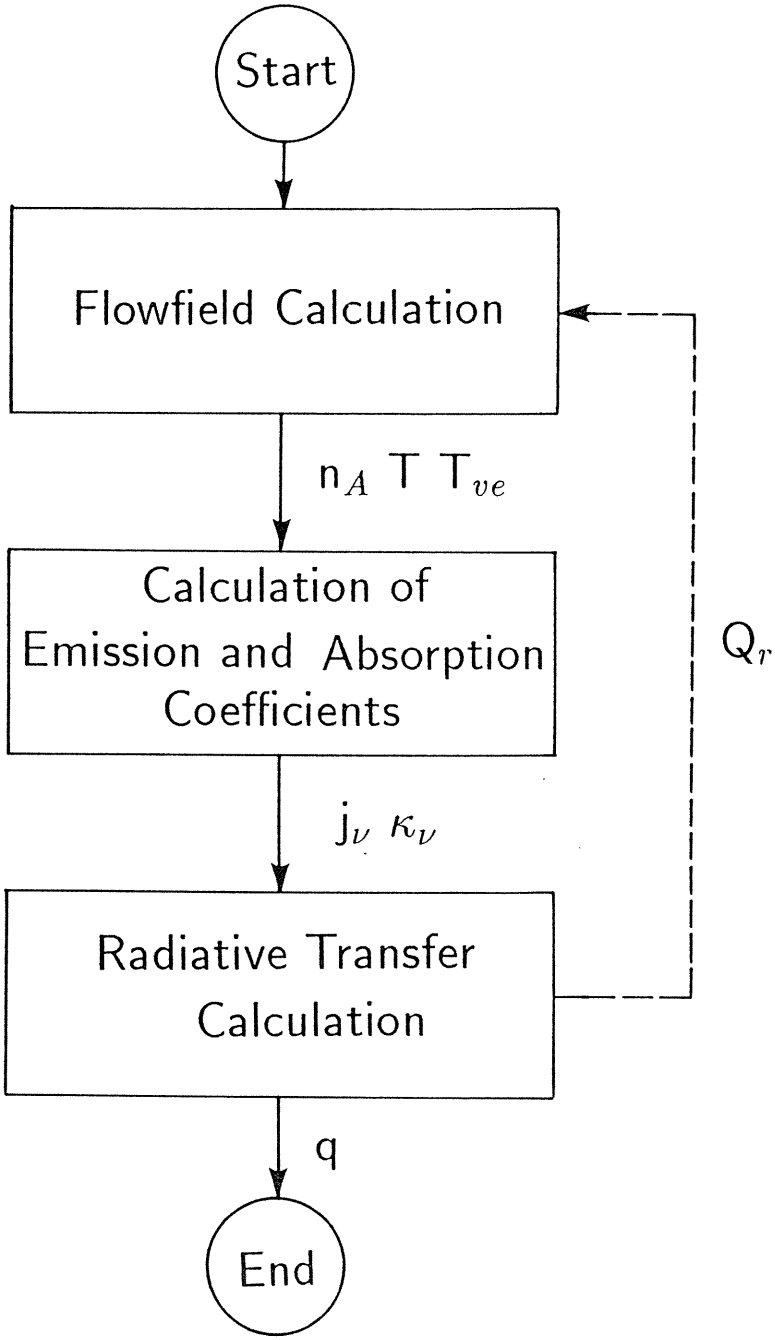

Fig. 5. 1. Flow chart of calculation.

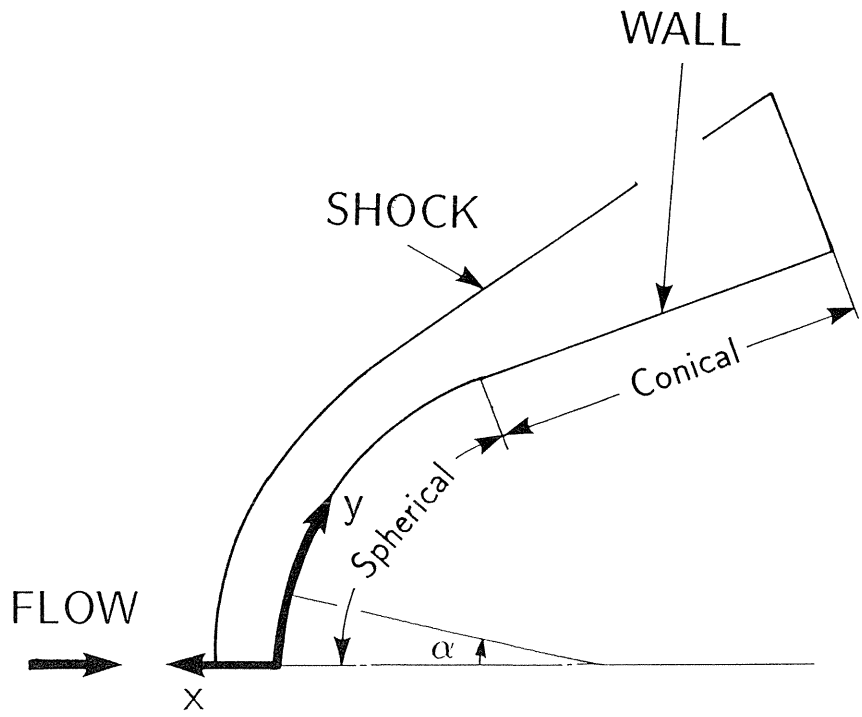

Fig. 5. 2. Blunt body.

The upstream and wall conditions are shown in Table 5.1. The flight Mach number ranges from 25 to 35. The corresponding flight velocity is 7.4 to 10.4 km/s. Note that the flight velocity is lower than that calculated from a Mach number based on the temperature at a zero altitude because the atmospheric temperature at 70 km altitude is lower. Although the wall temperature is practically determined by the thermal design of a vehicle, it is assumed to be uniform for simplicity.

The thermal radiation of the wall is not taken into account. The radiation incident on the wall is assumed to be totally absorbed; a purely abosrbing wall is assumed.

5. 3. *Distribution of Flowfield Properties*

The distributions of T and T_{ve} at a Mach number of 35 are shown in Fig. 5.3(a). Immediately behind the shock, since the energy relaxation between the (vibrational)-(electron translational) mode and the heavy particle (translational)-(rotational) mode is comparable with the flow resident time, T_{ve} is much lower than T. T_{ve} equals the upstream temperature at the shock front, then sharply rises, reaching its peak at around x=0.035 m. Such thermal nonequilibrium does affect the chemical reaction rates in this region. Since T is at a high level

Table 5. 1. Upstream and wall conditions.

Altitude	70 km
Upstream Pressure	5.5 Pa
Upstream Temperature	219 K
Flight Velocity	7.4 - 10.4 km/sec
Mach Number	25 - 35
Wall Temperature	1200 K
Wall Catalycity	non
Wall Reflectivity	0
Wall Absorptivity	1

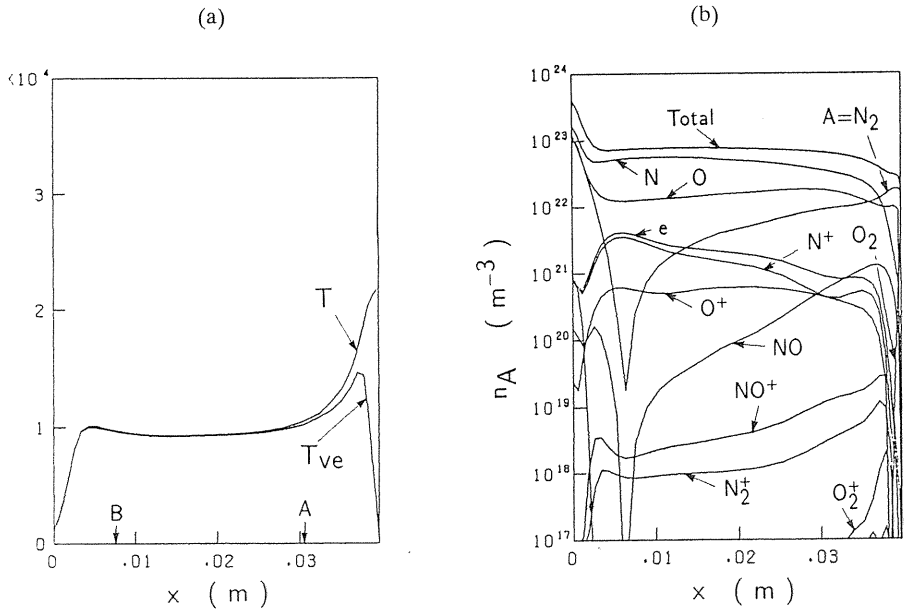

Fig. 5. 3. Distribution of (a) T and T_{ve}, (b) Number density, along the stagnation streamline (M=35).

there, chemical reactions including the dissociation and ionization of the molecules can take place at high rates. However, a dissociation rate and an associative reaction rate depend strongly on the vibrational temeprature. Moreover, an electron impact ionization rate depends totally on the electron translational temperature. Hence, T_{ve} does play an important role on the chemical reaction rates in this nonequilibrium region.

In the downstream region of x=0 to 0.03 m, these two temperatures are almost equal (thermally equilibrium region). Also, the chemical reactions become close to equilibrium. O_2 is almost fully dissociated. At a high Mach number of 35, N_2 is also dissociated to a large extent (see Fig. 5.3(b)). In the downstream region, the shock layer is composed mainly of atomic species. The electron number density is also high. The degree of ionization is as high as 5×10^{-2}. Of the ionized species, N^+ and O^+ are most populated. Due to high rates of the molecular dissociations, the number density of N_2^+, which, as will be shown later, is one of the major radiators, is not higher than that at Mach number of 25 (Fig. 5.4(b)).

In the vicinity of the wall, there is a thermal boundary layer in which the temperatures decreases from 10,000 to 1200 K (the wall temperature). The pressure in the shock layer is almost constant— about 1×10^4 Pa. Hence, according as the translational temperature decreases, the total number density sharply increases in the thermal boundary layer. However, due to high rates of recombination, the number densities of ionized species once decrease, resulting in a slight increase in temperature at the edge of the thermal boundary layer.

At Mach number 25 (Figs. 5.4(a),(b)), the chemical reacitons are almost in equilibrium in the region where the temperatures are almost constant. In this case, the degree of ionization is 2×10^{-3} at most. The most densely populated ionic species is NO^+. While O_2s are almost fully dissociated also in this case, less than half of N_2s are dissociated.

As can be predicted by the fluid dynamics of a perfect gas, the thickness of the shock layer decreases with the Mach number. This tendency is enhanced by endothermic chemical reactions whose rates increase with the Mach number.

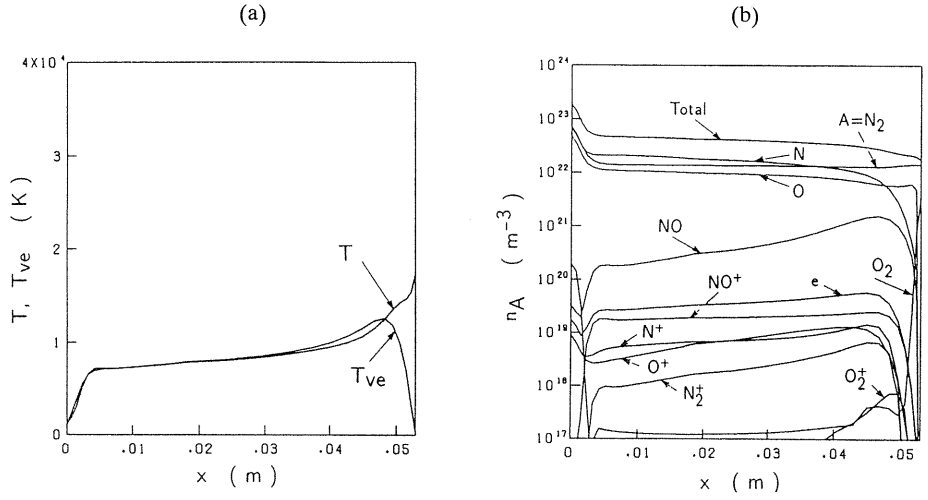

Fig. 5. 4. Distribution of (a) T and T_{ve}, (b) Number density, along the stagnation streamline (M=25).

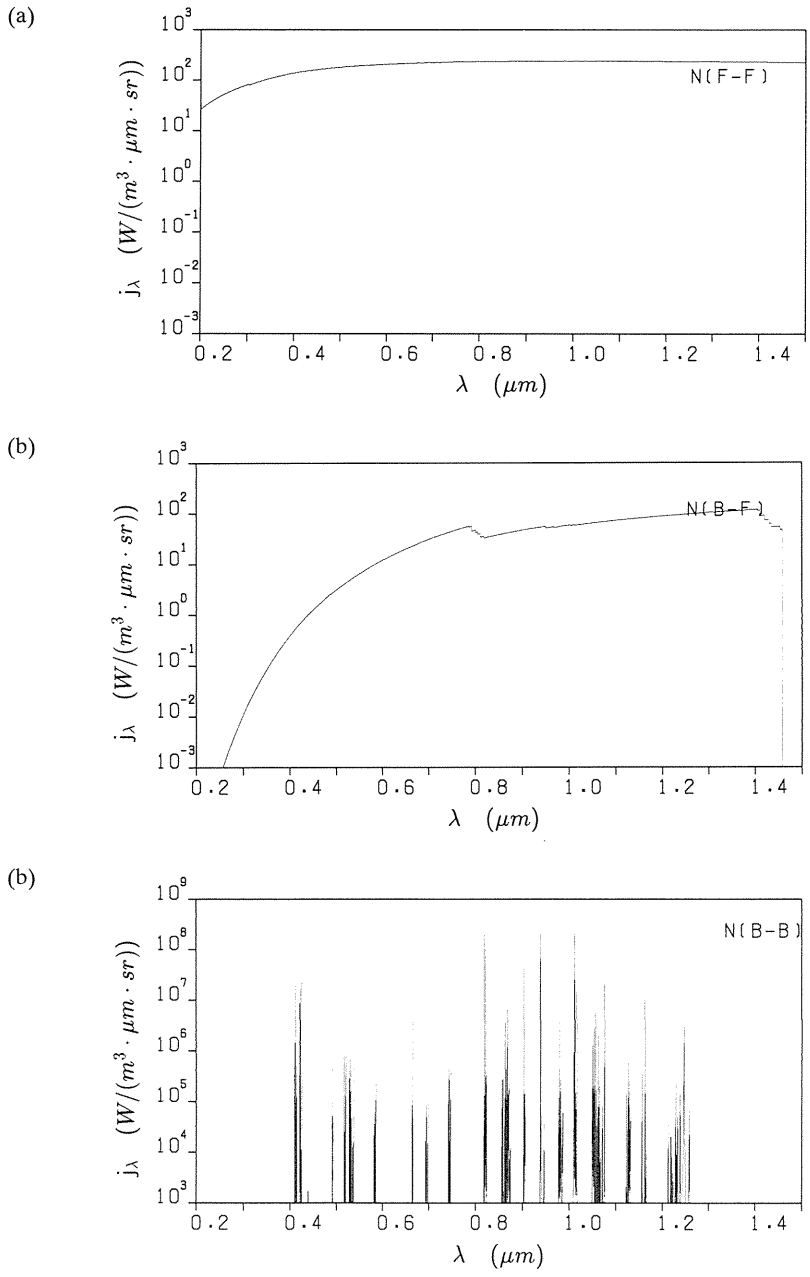

Fig. 5. 5. Examples of spectra (point A in Fig. 5.3(a)); (a) N (bound-bound transition), (b) N (bound-free transition), (c) N^+ (free-free transition), (d) O (bound-bound transition), (e) N^+_2 (first negative band), (f) N_2 (first positive band), (g) N_2 (second positive band), (h) NO (β band), (i) NO (γ band), (j) O_2 (Shumann-Runge band), (k) Total emission coefficient, (l) Total absorption coefficient.

(d)

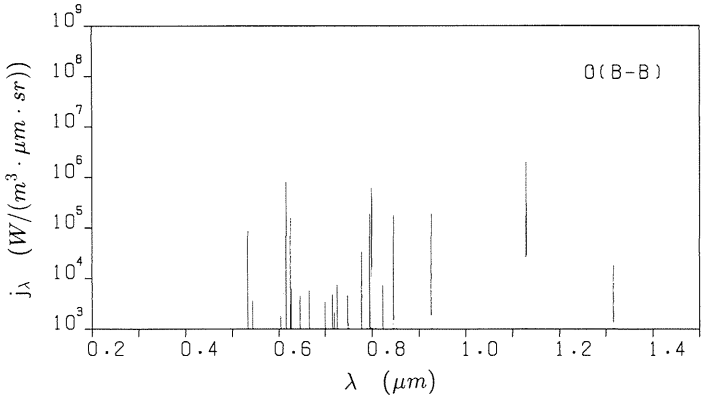

(e)

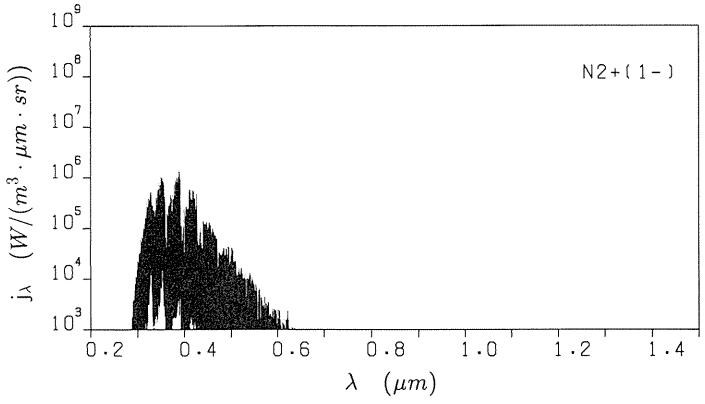

(f)

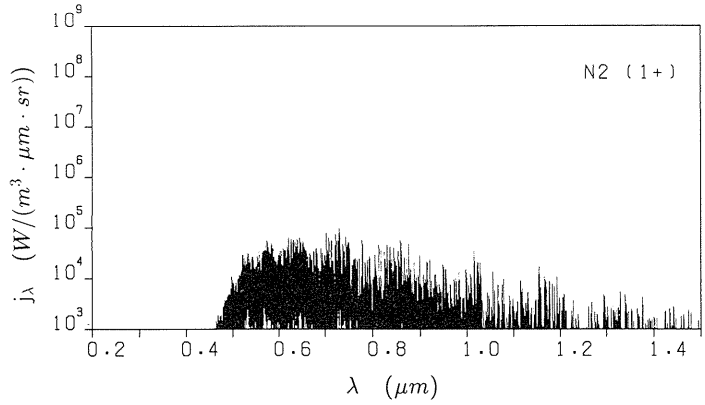

Fig. 5. 5. Examples of spectra (point A in Fig. 5.3(a)); (a) N (bound-bound transition), (b) N (bound-free transition), (c) N^+ (free-free transition), (d) O (bound-bound transition), (e) N^+_2 (first negative band), (f) N_2 (first positive band), (g) N_2 (second positive band), (h) NO (β band), (i) NO (γ band), (j) O_2 (Shumann-Runge band), (k) Total emission coefficient, (l) Total absorption coefficient.

(g)

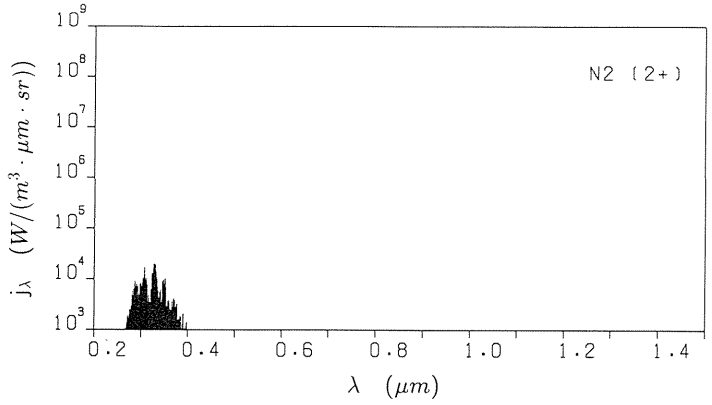

(h)

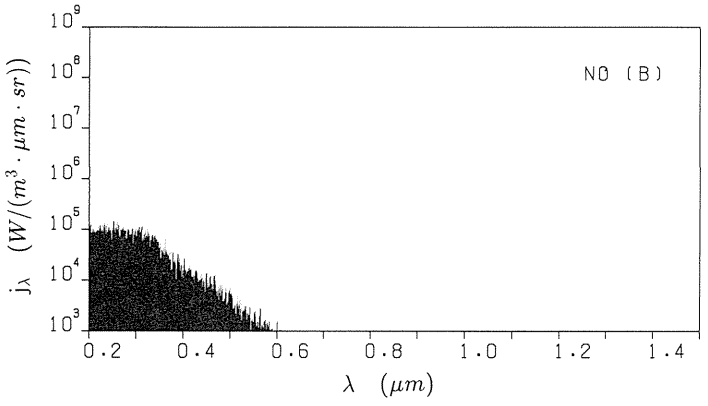

(i)

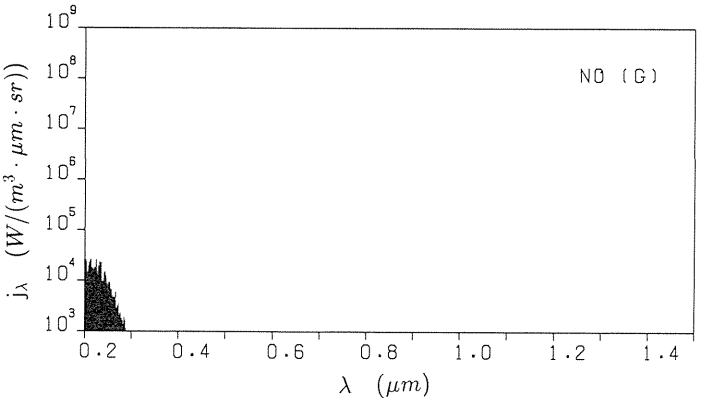

Fig. 5. 5. Examples of spectra (point A in Fig. 5.3(a)); (a) N (bound-bound transition), (b) N (bound-free transition), (c) N^+ (free-free transition), (d) O (bound-bound transition), (e) N^+_2 (first negative band), (f) N_2 (first positive band), (g) N_2 (second positive band), (h) NO (β band), (i) NO (γ band), (j) O_2 (Shumann-Runge band), (k) Total emission coefficient, (l) Total absorption coefficient.

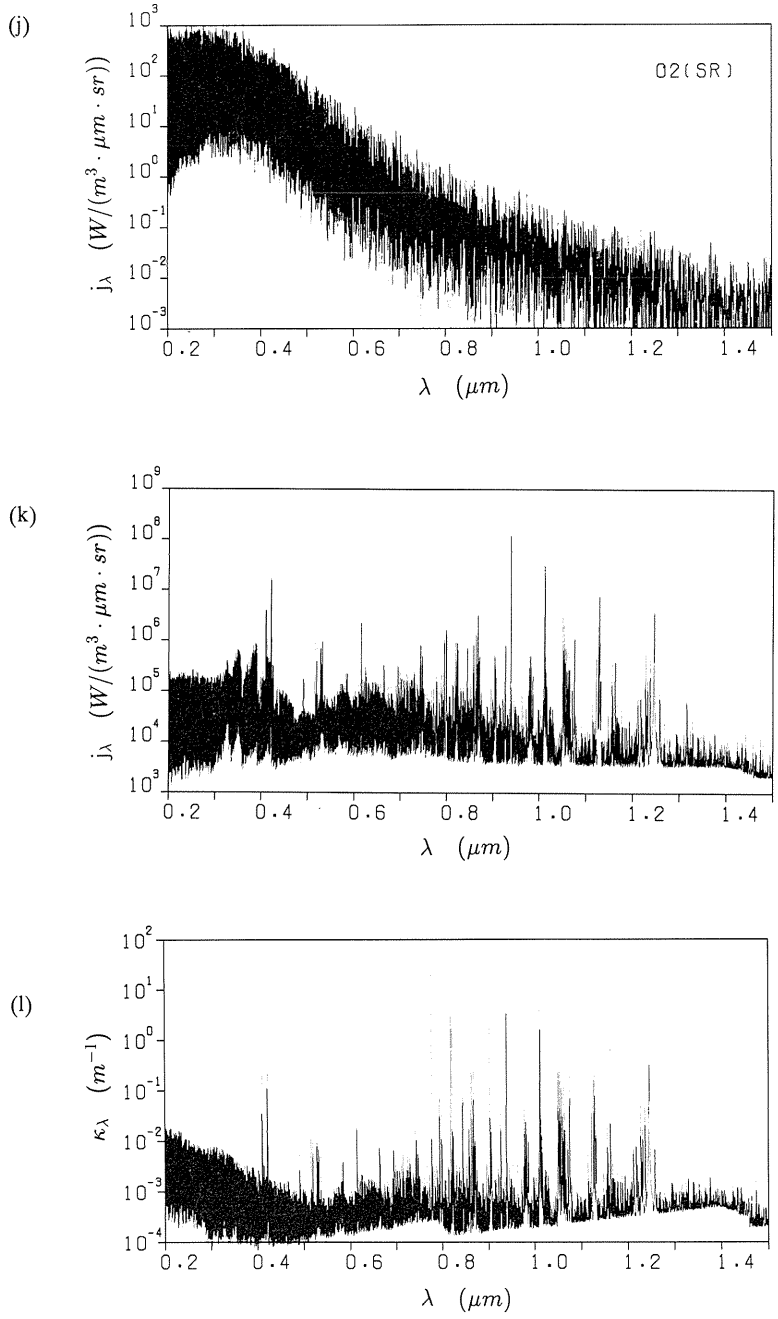

Fig. 5. 5. Examples of spectra (point A in Fig. 5.3(a)); (a) N (bound-bound transition), (b) N (bound-free transition), (c) N^+ (free-free transition), (d) O (bound-bound transition), (e) N^+_2 (first negative band), (f) N_2 (first positive band), (g) N_2 (second positive band), (h) NO (β band), (i) NO (γ band), (j) O_2 (Shumann-Runge band), (k) Total emission coefficient, (l) Total absorption coefficient.

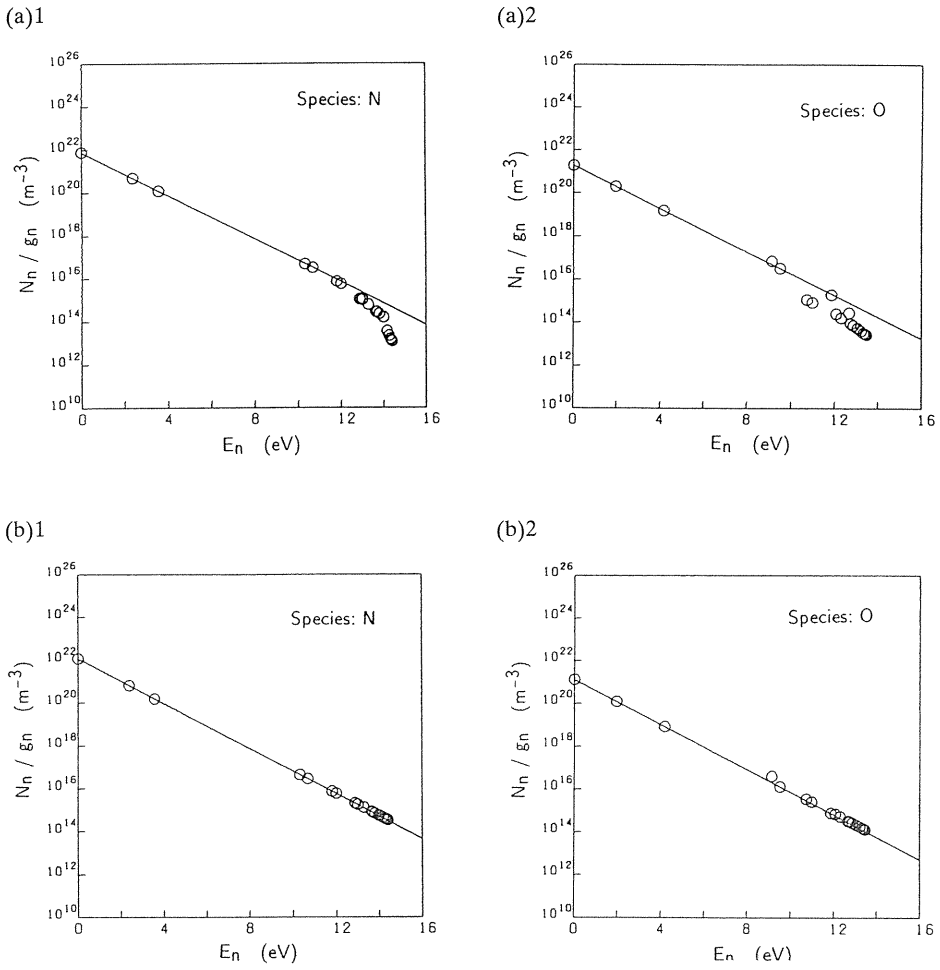

Fig. 5. 6. Boltzmann plots of atoms; 5.6(a) at point A in Fig. 5.3(a), 5.6(b) at point B in Fig. 5.3(a), — 1; N, 2; O. The solid lines represent Saha equilibrium.

5. 4. Examples of Spectra

Figures 5.5(a)-(j) show the spectra of the respective species. The spectra of the total emission coefficient are shown in Fig. 5.5(k). Those of the absorption coefficient by all the species are shown in Fig. 5.5(l). From 0.4 to 1.3 μm, atomic line spectra are observed ((a) and (d)). These spectra are very intense and are dominant in radiative emission power (see Fig. 5.7) in spite of their narrow line widths.

The spectrum by atomic bound-free transitions (b) has 'saw teeth' shape; Although the electronic bound energy levels are discretely disbributed, the free-electron translational energy distribution is continuous. Hence, such spectra are obtained.[5)]

Spectrum by free-free transitions (bremsstrahlung, (c)) is continuous. Since the electron density is at a low level there, this spectrum is relatively low. However, the radiative power of the spectrum varies in proportion to the square of electron density, and with weak dependence on temperature.[5] Hence, it becomes strong in the downstream region (see Fig. 5.7(a)).

From 0.3 to 0.6 μm, N_2^+ first negative band is observed. The upper electronic level $B^2\Sigma_u^+$, lies at a relatively low energy level -3.16 eV higher than the ground level. Therefore, the number density at the upper level is appreciably high, and the spectrum is a strong one in spite of low number density of N_2^+. Actually, it is one of the strongest spectra.

In Fig. 5.5(l), the upper line of the graph corresponds to the condition that the optical thickness for the maximum length of the volume element is almost unity. As seen in the figure, the condition $\kappa_\nu L << 1$ is satisfied in the whole wavelength range. This holds for all volume elements of the present calculation. Hence, it is seen that the method of calculating radiative transfer described in Chap. 4 is applicable to the present calculation.

5. 5. *Nonequilibrium Electronic Profile*

Figures 5.6 show Boltzmann plots of N and O. Figures 5.6.(a) show the plots in the thermal nonequilibrium region. In this region, the electron density is not high enough to equilibrate the electronic modes. Due to spontaneous radiative transitions, an atom or molecule at a high electronic level is de-populated in comparison with Saha equilibrium (the straight lines). In Eq. 85, the second terms in the parentheses, which are independent of the electron density, are appreciably large in comparison with the others.

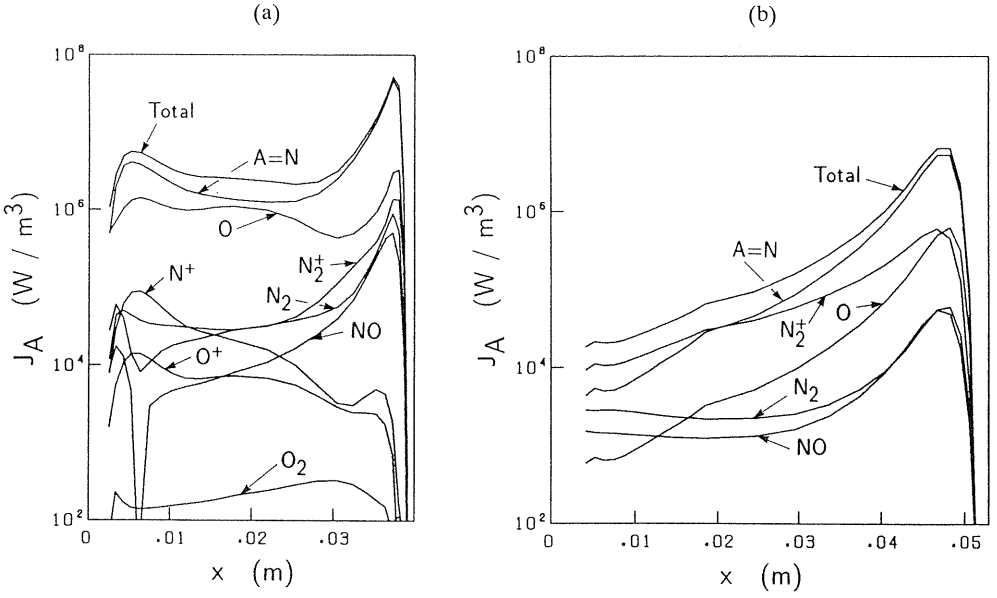

Fig. 5. 7. Distribution of emission power along stagnation streamline; (a) M=35 (b) M=25.

(a)

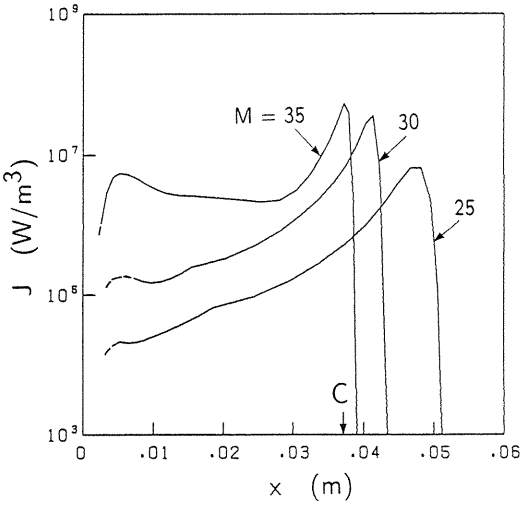

(b)

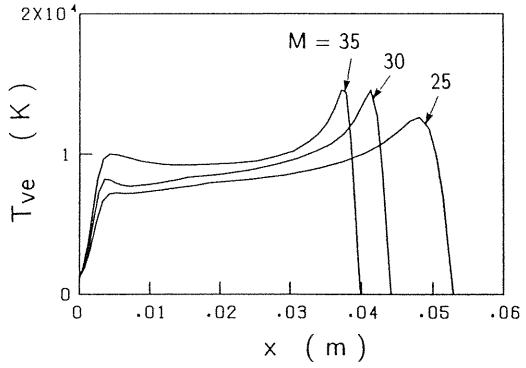

(c)

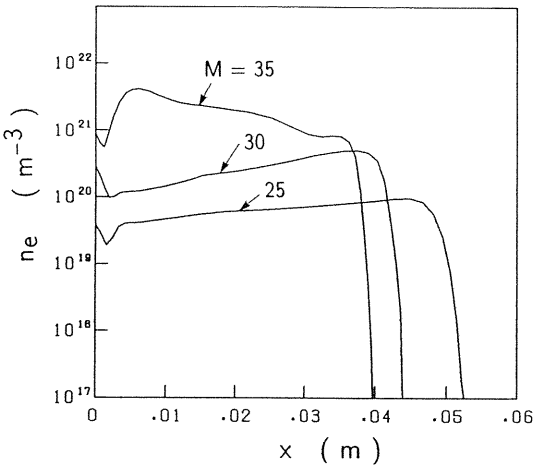

Fig. 5. 8. Distribution of (a) Total emission power, (b) Electron temperature, (c) Electron number density along stagnation streamline.

However, at point A in Fig. 5.3(a), T_{ve}, which is identical to the electron translational temperature, is as high as 14000 K. Hence, the number densities of highly excited particles are high. This tendency is prominent, in particular, in atomic species. In an atom, electronic energy levels are discretely distributed. In order to excite a nitrogen atom into a high level, for example, a large energy of more than 6 eV is necessary. The number density of the atoms which have such a high translational energy is sensitive to T_{ve}. As a result, in this high T_{ve} region, radiative emissions by N and O are dominant.

In thermal equilibrium region (point B in Fig. 5.3(a)), the distribution of the number densities are close to Saha equilibrium. In this region, electron density is at a high level. The first terms in the parentheses in Eq. 85 are large enough to dominate over the second ones.

5. 6. *Structure of Radiative Field*

Figures 5.7 show the distributions of the emission power by each species along the stagnation streamline. It is found that N, O and N_2^+ are dominant in emission power. The emission power by N_2^+ is due to the first negative band. Since the number density of O_2 is, as shown in Figs. 5.3(b) and 5.4(b), at low levels, its emission power is almost negligible.

The emission powers by ionized atoms become high a M=35, while they are negligible at M=25. Their radiative emission is due to free-free transitions (bremsstrahlung). The emission power by bremsstrahlung is proportional both to the number density of ions whose electric field decelerate an electron, and to the number density of electrons which are decelerated with radiative emission. At a temperature of the order of 10^4 K, one can neglect the effect of multiple ionization. Hence, the emission power is proportional to the square of the electron number density. As seen in Fig. 5.8(c), the electron number density at M=35 is a couple of orders in magnitude higher than that at M=25. Therefore, the emission by the ions vastly increases with the Mach number.

At point C at Mach number 35 in Fig. 5.8(a) where the emission power is maximum,

$$\frac{[\text{characteristic time of radiative energy emission}]}{[\text{characteristic flow resident time}]} = \frac{e/P}{\Delta x/v} \tag{99}$$

is calculated to be 270. It follows that the effect of radiative energy emission on the total energy conservation of the flow can be neglected under the present condition.

5. 7. *Radiative Heat Transfer over Wall*

Using the method described in Chap. 4, the radiative heat transfer over the blunt body is calculated (Fig. 5.9). The radiative heat transfer is highest at the stagnation point. It sharply increases with the Mach number. At a high Mach number, the region where T_{ve} is at a high level extends to the downstream region. Hence, the width at half-height of radiative heat transfer increases with the Mach number. At M=35, the temperatures around the conical part of the blunt body also become at high levels, resulting in heat transfer which can not be neglected.

As seen in Table 5.2, the radiative heat transfer more sharply increase with the Mach number than the convective one. The radiative heat transfer is sensitive to the temperature and density of electrons, both of which sharply increase with the Mach number (Figs. 5.8(b) and 5.8(c)). In contrast, due to endothermic reactions such as dissociation and ionization, the convective heat ransfer just gradually increases with the Mach number. At M=35, the radiative heat transfer becomes as high as 8.3×10^4 W/m^2, and comparable with the convective one. These results suggest that radiative heat transfer is far from negligible to the design of a reentry vehicle at a high flight Mach number.

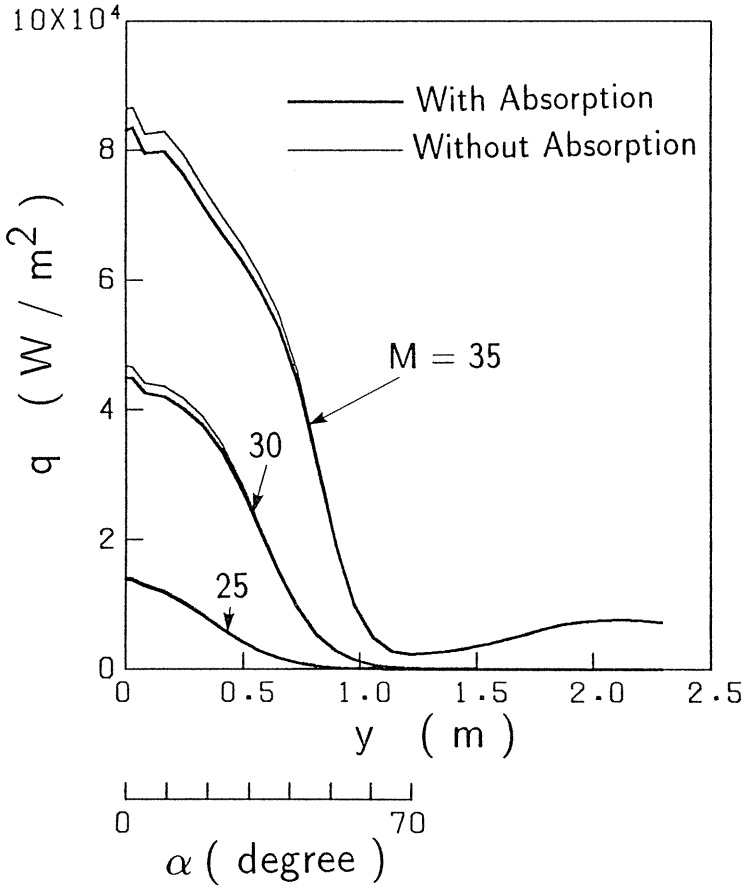

Fig. 5. 9. Distribution of radiative heat transfer along blunt body surface.

Table 5. 2. Comparison of radiative heat transfer with convective one at stagnation point [$\times 10^4$ W/m^2].

M	RADIATIVE	CONVECTIVE
25	1. 4	11. 6
30	4. 5	13. 8
35	8. 3	14. 7

6. Conclusion

In this paper, the method of calculating the radiative field in a hypersonic air shock layer has been developed. The band method with series-expansion approximation enables one to conduct wavelength-dependent, three-dimensional radiative transfer calculation in which the effect of self-absorption of gas is taken into account. The sample calculation suggests that at Mach numbers higher than 30, radiative heat transfer can be comparable with the convective one—far from negligible in the thermal design of a reentry vehicle.

References

1) London, H.S., "Changes of Satellite Orbit by Aerodynamic Maneuvering," Journal of the Aerospace Sciences, vol.29, March 1962, pp. 323-332.
2) Park, C., "Assessment of Two-Temperature Kinetic Model for Ionizing Air," Journal of Thermophysics and Heat Transfer, Vol. 3, No. 3, 1989, p. 233-244.
3) Walberg, G.D., "A Survey of Aeroassisted Orbit Transfer," Journal of Spacecraft and Rockets, Vol. 22, No. 1, 1985, pp. 3-8.
4) Howe, J.T., "Introductory Aerothermodynamics of Advanced Space Transportation Systems," Journal of Spacecraft and Rockets, Vol. 22, No. 1, 1985, pp. 19-26.
5) Zel'dovich, Y.B. and Raizer, Y.P.: *Physics of Shock Waves and High-Temperature Hydrodynamic Phenomena, Volume I*, Academic Press, New York, 1966.
6) Pai, Shih-I: *Radiation Gas Dynamics*, Springer-Verlag, New York, 1966.
7) Herzberg, G.: *Molecular Spectra and Molecular Structure; Volume I-Spectra of Diatomic Mlecules*, 2nd edition, Robert E. Krieger Publishing Co., Malabar, Florida, 1989.
8) Herzberg, G.: *Atomic Spectra and Atomic Structure*, Dover Publications, New York, 1944.
9) Wiese, W.L., Smith, M.W. and Glennon, B.M., "Atomic Transition Probabilities. Volume I, Hydrogen through Neon," National Standard Reference Data Series, NBS-4, 1966.
10) Arnold, J.O., Whiting, E.E. and Lyle, G.C., "Line by Line Calculation of Spectra from Diatomic Molecules and Atoms Assuming a Voigt Line Profile," Journal of Quantitative Spectroscopy and Radiative Transfer, Vol. 9, 1969, pp. 775-798.
11) Park, C., "Nonequilibrium Air Radiation (NEQAIR) Program: User's Manual," NASA TM-86707, 1985.
12) Park, C., "Calculation of Nonequilibrium Radiation in AOTV Flight Regimes," AIAA 84-0306, 1984.
13) Park C.: *Nonequilibrium Hypersonic Aerothermodynamics*, John Wiley & Sons, New York, 1990.
14) Griem, H.R.: *Plasma Spectroscopy*, McGraw-Hill, New York, 1964.
15) Lochte-Holtgreven, W. et al.: *Plasma Diagnostics*, North-Holland Publishing Company, Amsterdam, 1968.
16) Schadee, A., Journal of Quantitative Spectroscopy and Radiative Transfer, vol. 7, 1967, p. 169.
17) Lorentz, H.A., Versl. Amsterd. Akad. vol. 14, 1905, p. 577.
18) Penner, S.S.: *Quantitative Molecular Spectroscopy and Gas Emissivities*, Addison-Wesley, Reading, 1959.
19) Breene, R.G.Jr.: *The Shift and Shape of Spectral Lines*, Pergamon Press, Longdon, 1961.
20) Ch'en, S. and Takeo, M., "Broadening and Shift of Spectral Lines Due to the Presence of Foreign Gases," Reviews of Modern Physics, Vol. 29, No. 1, 1957, pp. 20-73.
21) Panofsky, W.K.H. and Phillips, M.: *Classical Electricity and Magnetism*, Addison-Wesley Publishing Company, Cambridge, 1961.
22) Sasoh, A., Chang, X. and Fujiwara, T., "Equilibrium and Nonequilibrium Radiation Heat Transfer over a Reentry Blunt Body, AIAA paper 90-2113, July 1990.

23) Edwards, D.K., "Molecular Gas Band Radiation," Advance in Heat Transfer, vol. 12, 1976, pp. 115-193.
24) Murayama, T. and Fujiwara, T., "Thermally and Chemically Nonequilibrium Hypersonic Flow in Three-Dimensional Geometry," Proceedings of the 17th International Sysmposium on Space Technology and Science, Tokyo, May 1990.
25) Reddy, K.V., Fujiwara, T., Ogawa, T. and Arashi, K., "Computation of Three-Dimensional Chemically Reacting Viscous Flow around Rocket Body," ISAS Report, SP-7, November 1988, pp. 39-71.
26) Reddy, K., Fujiwara, T. and Murayama, T., "Thermally and Chemically Nonequilibrium Flow Analyzed by Park's Two-Temperature Model," AIAA paper 90-0142, January 1990.
27) Murayama, T., Sasoh, A. and Fujiwara, T., Proceedings of Symposium on Shock Waves, Japan '90, Tokyo, Dec. 1990, pp. 361-366.
28) Park, C., "Assessment of Two-Temperature Kinetic Model for Ionizing Air," Journal of Thermophysics and Heat Transfer, Vol. 3, No. 3, 1989, pp. 233-244.
29) Millikan, R.C. and White, D.R., "Systematics of Vibrational Relaxation," Journal of Chemical Physics, Vol. 139, 1963, pp. 3209-3213.
30) Yos, J.M., "Transport Properties of Nitrogen, Hydrogen, Oxygen and Air to 30,000 K," Technical Memorandum RAD TM-63-7, AVCO-RAD, Wilmington, 1963.
31) Lee, J.H., "Basic Governing Equations for the Flight Regimes of Aeroassisted Orbital Transfer Vehicles," Progress in Astronautics and Aeronautics, Vol. 96, 1985, pp. 3-53.

Appendix; Approximation of Rotational Energy

In this study, the rotational energy is approximated as follows:

1. $^2\Pi \leftrightarrow {}^2\Sigma$ transition (NO γ band)

In this case, the effect of spin splitting[7] is taken into account.

For $J = K + \frac{1}{2}$,

$$F_1(J) = B_v[(J+\tfrac{1}{2})^2 - \Lambda^2 - \tfrac{1}{2}\{4(J+\tfrac{1}{2})^2 + Y(Y-4)\Lambda^2\}^{\frac{1}{2}}] \ . \tag{100}$$

For $J = K - \frac{1}{2}$,

$$F_2(J) = B_v[(J+\tfrac{1}{2})^2 - \Lambda^2 + \tfrac{1}{2}\{4(J+\tfrac{1}{2})^2 + Y(Y-4)\Lambda^2\}^{\frac{1}{2}}] \ . \tag{101}$$

2. Other transitions

For other transitions, the effect of spin splitting is ignored. The following approximation is made:

$$F(J) = B_v[(J(J+1) + 4Z_2] - D_v(J+\tfrac{1}{2})^4 \ , \tag{102}$$

Here, for $\Delta\Lambda=0$ triplet (S=1),

$$Z_2 = \frac{1}{3Z_1}\left[\Lambda^2 Y(Y-1) - \frac{4}{9} - 2J(J+1)\right] , \tag{103}$$

$$Z_1 = \Lambda^2 Y(Y-4) + \frac{4}{3} + 4J(J+1) \tag{104}$$

$$Y = \frac{A}{B_v} . \tag{105}$$

For the others,

$$Z_2 = 0 . \tag{106}$$

A is a coupling constant which is a measure of the strength of the coupling between the spin **S** and the orbital angular momentum Λ.

In this study, the effect of Λ-coupling is ignored. The further details are described in Refs. 7), 10) and 11).